NASA Technical Memorandum 4372

Structural Performance of Two Aerobrake Hexagonal Heat Shield Panel Concepts

John T. Dorsey
Langley Research Center
Hampton, Virginia

James W. Dyess
Virginia Polytechnic Institute and State University
Blacksburg, Virginia

National Aeronautics and Space Administration

Office of Management

Scientific and Technical Information Program

1992

Abstract

Structural sizing and performance are presented for two structural concepts for an aerobrake hexagonal heat shield panel. One concept features a sandwich construction with an aluminum honeycomb core and thin quasi-isotropic graphite-epoxy face sheets. The other concept features a skin-rib isogrid construction with thin quasi-isotropic graphite-epoxy skins and graphite-epoxy ribs oriented at 0°, +60°, and −60° along the panel. Linear static, linear bifurcation buckling, and nonlinear static analyses were performed to compare the structural performance of the two panel concepts and assess their feasibility for a lunar transfer vehicle aerobrake application.

Introduction

There is great interest in manned exploration of the solar system, beginning with a return to the Moon and followed by a manned mission to Mars (ref. 1). Since the vehicles required for these missions are too large and massive to be placed in orbit by a single launch of the Space Shuttle or a heavy-lift launch vehicle, some on-orbit assembly and construction will likely be required (ref. 2). A large portion of the mass of the lunar transfer vehicle (LTV) and the Mars transfer vehicle (MTV) consists of the propellant required for propulsive braking. Aerobraking, which uses aerodynamic drag forces (created during an aeropass through a planetary atmosphere), can be used as an alternative to propulsive braking to achieve the reduction in velocity required to enter orbit around a planet. Thus, by reducing the amount of propellant required for a mission, aerobraking provides a potentially effective way to reduce the initial mass of lunar and Mars transfer vehicles (refs. 3 and 4).

For LTV's and MTV's that use aerobraking, spacecraft components are packaged on the leeward side of the aerobrake, as shown in figure 1, so that the aerobrake protects the components from the extreme thermal environment generated during the aeropass. The aerobrake design selected for a particular mission will be influenced by many parameters, including the total mass of the spacecraft, maximum deceleration rate limit (crew physiological requirement), maximum allowable stagnation temperature (thermal protection requirements), and lift-to-drag ratio required (to maintain control). In order for an aerobrake to be viable for a mission, it must be lightweight; have minimal packaged volume for transporting to low Earth orbit; be easily constructed on orbit; and in some cases, be reusable.

One aerobrake structural concept that is designed to be constructed on orbit and has received considerable attention is presented in references 5 and 6. This aerobrake is 120 ft in diameter and was sized for an MTV having a total spacecraft mass of 450 000 lbm. This concept consists of a lightweight tetrahedral truss with hexagonal heat shield panels that are attached to the truss at discrete points (see fig. 2(a)). Because sandwich panels are very efficient from a structural performance and mass standpoint, the hexagonal panels studied in these references used sandwich construction. Equations are presented in references 5 and 6 for sizing minimum mass sandwich panels based on a transverse pressure load and a maximum deflection criterion.

An isogrid structural concept is also considered for the heat shield panels because isogrid construction can result in lightweight panel designs (ref. 7). In addition, there may be other nonstructural considerations that make the isogrid structural concept an attractive alternative to the sandwich design. For example, the open structure of the isogrid allows the load-carrying ribs to be easily inspected for damage before certifying a reusable aerobrake for the next mission. Additional structure required to accommodate loads introduced at the panel support points may be minimized because connections can be made at the isogrid rib intersections. This can be contrasted with sandwich panels, where mass advantages predicted from feasibility studies are "often lost in the reduction to design practice, especially in the design of joints and attachments" (ref. 8). Another potential problem with sandwich panels is that aerobrake heating may lead to large temperature differences between the front and back faces of the sandwich panel. This temperature differential can cause differential expansion and contraction in the two face sheets, which can place the core material under tension, and if sufficient stress is generated, separate the face sheets from the core (ref. 9).

Thus, it is worthwhile to study the feasibility of the isogrid panel concept as an alternative to the sandwich concept at an early stage of the aerobrake design process. In this paper, results are presented for both the sandwich and isogrid panel concepts. Two of the four panel-to-truss attachment concepts studied in reference 6 are used in this study (see fig. 2(b)). These attachment concepts were chosen because they result in the largest and smallest masses per unit area for the sandwich panel. The preliminary design methods presented in reference 6 are used in the present study to size sandwich panels for an LTV aerobrake (which is 45 to 50 ft in diameter). Results that are representative of the mass and

performance that can be obtained for the isogrid panel concept are presented and can be used to assess the feasibility of the isogrid concept for an aerobrake application. If the performance and mass penalties for isogrid construction are determined to be small compared with a sandwich design, then a more in-depth study of the isogrid concept will be warranted.

An important limitation of the previous studies has been that the heat shield panels are designed using only a global panel structural deflection criterion. However, a more important design consideration for some thermal protection systems, such as the tiles on the Space Shuttle, is the local curvature in the structure over the length of the tile. In order to relate thermal protection system (TPS) deflection limits to the panel design, equations are derived in the present paper to calculate from a set of transverse displacements the local radius of curvature (ROC) induced in the panel. These equations establish one possible relationship between local panel curvature and TPS tile size and deflection limits.

Nomenclature

A	area, in^2
c_1, c_2, c_3	constants in equation (5)
D	panel bending stiffness, in-lbf
d	panel diameter, in.
E	Young's modulus, lbf/in^2
F	rib frequency (see eq. (4))
G	shear modulus, lbf/in^2
h	height, in.
L	length, in.
L_{rib}	total rib length, in.
M	mass, lbm
N	membrane stress, lbf/in.
n	number of 0° plies in rib laminate
p	pressure
R	radius, in.
ROC	radius-of-curvature, in.
t	thickness, in.
w	displacement normal to panel surface, in.
w_a, w_b, w_c	normal displacements associated with points a, b, and c, in.
$w_{\max}$	maximum normal panel displacement, in.
x, y, z	orthogonal coordinate system in three-dimensional space
α	panel coefficient (see eq. (12))
θ	circumferential direction
ν	Poisson's ratio
ρ	material density, lbm/in^3

Subscripts:

c	core
eff	effective
f	face sheet
HP	hexagonal panel
IP	isogrid panel
mm	minimum mass
R	radial direction
rel	skin center relative (displacement)
rib	isogrid ribs
s	symmetric lay-up about the midplane
sk	isogrid skin
SP	sandwich panel
tcs	triangular cell size
$TPS, 1$	thermal protection system tile size 1
x, y	laminate axes (x is along the fiber)
θ	circumferential direction

Hexagonal Heat Shield Panel Design Concepts

In this study the aerobrake, which is part of an LTV, has an overall diameter of 44 ft (see ref. 10). The heat shield panels are attached to nodes on the windward face of the tetrahedral truss (see fig. 2(a)) and function as a continuous aerobraking surface. The heat shield panels are assumed to be flat to simplify the preliminary design process as in references 5 and 6. The TPS used on the heat shield panels could be ablative material or reusable tiles, depending on the specific mission requirements; the TPS is applied to one face of the structural panel as shown in figure 3. Any additional structural stiffness (which is assumed to be small) provided by the TPS is also neglected to simplify the preliminary design process. In this section, general design considerations for hexagonal heat shield panels will first be discussed, followed by specific design details for the sandwich and

isogrid panel concepts. Finally, a methodology for sizing TPS tiles based on a local structural radius of curvature will be examined.

Design Considerations

There are several design considerations associated with the hexagonal heat shield panels. In reference 6, it is shown that the size and dimensions of the hexagonal heat shield panel are determined primarily by the aerobrake diameter, the number of rings in the tetrahedral support truss, and the panel support locations. In the present study, the hexagonal panels are also constrained to fit inside the cargo bay of the Shuttle Space Transportation System, which limits the panel diameter to a maximum of 14 ft. The largest possible diameter panel is desired because it minimizes the truss and panel part counts and thus reduces the amount of on-orbit construction required. The largest panel permissible with panel support concept A has a diameter of 121.13 in. and attaches to a 2-ring support truss. Similarly, the largest panel permissible with support concept D has a diameter of 150.34 in. and attaches to a 3-ring support truss.

Although the actual aerodynamic pressure distribution acting on the aerobrake during reentry is nonuniform, a uniform distribution is assumed to simplify the preliminary design process. The magnitude of this uniform pressure is derived from the aerobrake inertia force due to a constant deceleration rate. For a spacecraft mass of 25 500 lbm, a $5g$ maximum deceleration rate, a cross-sectional area of 219 000 in^2, and a factor of safety of 1.4, equation (1) from reference 6 gives a pressure load of 0.815 psi, which is applied normal to the plane of the panel.

Sandwich Panel Description

The sandwich panels used in the present study feature an aluminum honeycomb core and graphite-epoxy face sheets (see fig. 3). The honeycomb core has a density ρ_c of 0.00231 lbm/in^3 (4.0 lbm/ft^3), and the graphite-epoxy material used in the face sheets has the following lamina properties: $E_x = 40.8 \times 10^6$ psi, $E_y = 1.0 \times 10^6$ psi, $G_{xy} = 0.6 \times 10^6$ psi, $\nu_{yx} = 0.3$, and a ply thickness of 0.005 in. The face sheets are quasi-isotropic, resulting in an effective laminate modulus E_{eff} of 14.4×10^6 psi and a material density ρ_f of 0.063 lbm/in^3. Minimum gauge for the face sheets was assumed to be 0.04 in.; this resulted from an 8-ply mid-plane symmetric, quasi-isotropic laminate.

Isogrid Panel Description

The isogrid pattern chosen for the hexagonal heat shield panels consists of equilateral triangles, as shown in figure 4(a). Using ribs oriented at 0°, +60°, and −60° results in overall isotropic membrane stiffness properties for the panel. The number of equilateral triangular cells along each edge of the hexagonal isogrid panel is defined as the frequency F of the panel. A cross section of the isogrid panel is shown in figure 4(b). In the present study, the ribs are assumed to be blade stiffeners, as shown in the figure. A fixed ratio of height (h_{rib}) to thickness (t_{rib}) is chosen for the ribs to reduce the number of independent variables in the feasibility study. Based on discussions with senior engineers, a rule-of-thumb value of 6 was chosen for this ratio. The material used in the isogrid panel has the same properties as the graphite-epoxy used in the skins of the sandwich panel. A quasi-isotropic laminate is assumed for the skin, resulting in an effective laminate modulus of 14.4×10^6 psi. The ribs are designed to carry most of the loading in the panel, and thus a laminate that maximizes the rib extensional modulus is desirable. The rib design chosen, a $[+45, -45, 0_n]_s$ lay-up, uses a pair of ±45° plies to stabilize the 0° plies that run along the longitudinal axis of the rib. Representative values of n, together with the resulting total number of plies in the rib, the total rib thickness, and the rib effective laminate modulus, are tabulated in table I.

Since the attachment points for support concept A are at vertices of the hexagonal panel, no complications arise as the rib frequency is varied. However, with support concept D the attachment points are in the interior of the panel two-thirds of the distance from the panel center to the edge of the hexagon (see fig. 4(c)). When the rib frequency is an integral multiple of 3, there will be an intersection of ribs at these points, providing a stiff attachment or support point for the panel. For all other rib frequencies, the support points will fall in the interior of a triangular cell, leading to a very "soft" support point. In these cases, three additional members are added to the isogrid pattern to provide attachment points on ribs, as illustrated in figure 4(c) for the case of $F = 2$.

TPS Tile Sizing

In general, TPS tiles such as those used on the Shuttle are very fragile and are separated from the underlying structure by a strain isolation pad (SIP). However, for a given tile size, there will exist a deflection limit in the underlying support structure that cannot be exceeded without causing the tile to separate from the structure because of failure of the SIP. A local induced radius of curvature can be calculated from transverse panel deflections, as shown in figure 5(a), and then related to an allowable tile

deflection (w_{TPS}) and tile size (L_1, L_2), as illustrated in figure 5(b). Two design approaches for the structural/TPS system are possible. In the first approach, the structure is designed without regard for TPS deflection constraints, and once the type of TPS tile and its maximum allowable deflection are specified, a maximum tile size can be calculated. In the second approach, a required TPS tile size and a maximum allowable deflection are specified, and the structure is designed with sufficient stiffness such that the minimum induced ROC of the panel is acceptable for the TPS design. In general, a larger minimum ROC implies a flatter deflected structure, which should allow more freedom in the TPS design process.

Analysis

This section describes the methods used to size the sandwich and isogrid hexagonal panels. The Engineering Analysis Language (EAL) finite element program was used to model and analyze the sandwich and isogrid panels (see ref. 11). The equations that relate normal panel displacements to an induced radius of curvature are also derived.

Sandwich Panel Model

Equations (28) and (29) in reference 6 are used to design the sandwich panels with support concepts A and D. The finite element discretization used for the sandwich panel models is identical to that found in reference 6 and is illustrated in figure 6.

Isogrid Panel Model

Geometry. The isogrid panel skin was discretized into a uniform triangular-element pattern, as shown in figure 7, so that the resulting element boundaries would lie along rib lines. The isogrid panel skin is modeled with triangular plate elements, and the ribs are modeled with beams with a rectangular cross section. In order to correctly model the rib stiffness, the rib neutral axis is offset from the skin neutral axis by a distance equal to half the skin thickness plus half the rib height, as shown in figure 7.

Design procedure. The approach used to size an isogrid panel was to choose a panel mass and determine the most structurally efficient way to distribute that mass between the ribs and the skin. Initially, sandwich panel designs were determined for each of the two panel diameters (one associated with support concept A, and one with support concept D) and their mass was taken as the total mass for the respective isogrid panel. Since mass is held constant, the most efficient isogrid panel is the one that gives the smallest deflection when subjected to the design load. The structural performance of the isogrid panel can then be compared with the performance of the sandwich panel having identical mass. Once the panel mass and planform area are specified, the design parameters that can be varied are the skin thickness, the total length of ribs, the rib thickness, and the rib height.

The total mass of the isogrid panel is

$$M_{IP} = \rho \left(A_{IP}\, t_{\mathrm{sk}} + L_{\mathrm{rib}}\, h_{\mathrm{rib}}\, t_{\mathrm{rib}} \right) \tag{1}$$

Since the rib height h_{rib} is chosen to be 6 times the rib thickness t_{rib}, the total mass of the skin stringer panel becomes

$$M_{IP} = \rho \left(A_{IP}\, t_{\mathrm{sk}} + L_{\mathrm{rib}}\, 6 t_{\mathrm{rib}}^2 \right) \tag{2}$$

where t_{sk} is the panel skin thickness and L_{rib} is the total length of ribs used in the panel. The area of the isogrid hexagonal panel (A_{IP}) is

$$A_{IP} = \frac{3\sqrt{3}}{8} d_{HP}^2 \tag{3}$$

For an isogrid panel, the number of subdivisions along a panel edge, or the rib frequency F, is a major design parameter and will determine the total length of ribs for the panel. The rib frequency, illustrated in figure 4(a), is defined by

$$F = \frac{d_{HP}}{2 L_{tcs}} \tag{4}$$

where d_{HP} is the hexagonal panel diameter and L_{tcs} is the length of the side of a triangular cell formed by the ribs. When a rib frequency is chosen for the panel, only two variables remain undefined in equation (2): the skin thickness and the rib thickness. Thus, a value of skin thickness can be chosen and the corresponding rib thickness calculated for a constant mass panel with equation (2). The effective modulus of the skin remains constant as the skin thickness (which is assumed to be a continuous function for this study) is varied. However, the modulus of the ribs will increase as the rib thickness is increased because a greater percentage of the rib laminae are oriented in the 0° direction (see table I).

Radius-of-Curvature Derivation

A general expression for relating three adjacent displacements on the analysis model to a local radius of curvature, as shown in figure 5(a), is desired. The three displacements are assumed to be coplanar and

equally spaced for this analysis. The general form for the equation of a circle (see ref. 12) is

$$y^2 + z^2 + c_1 y + c_2 z + c_3 = 0 \tag{5}$$

The locations of the three deflected points used to derive the ROC are point a: $y = -L$, $z = -w_a$; point b: $y = 0$, $z = -w_b$; and point c: $y = L$, $z = -w_c$. Substituting these three points into equation (5) results in three equations with the three unknown coefficients c_1, c_2, and c_3. The three equations were solved symbolically using the program Theorist (see ref. 13), with the following result:

$$c_1 = \frac{1}{2L}\left[-w_c^2 + w_a^2 + \frac{(w_c - w_a)\left(w_c^2 - 2w_b^2 + w_a^2 + 2L^2\right)}{w_c - 2w_b + w_a}\right] \tag{6}$$

$$c_2 = \frac{w_c^2 - 2w_b^2 + w_a^2 + 2L^2}{w_c - 2w_b + w_a} \tag{7}$$

$$c_3 = \frac{w_b\left[2L^2 + w_c\left(w_c - w_b\right) + w_a\left(w_a - w_b\right)\right]}{w_c - 2w_b + w_a} \tag{8}$$

The equation for the induced radius of curvature is

$$\mathrm{ROC} = \frac{1}{2}\sqrt{c_1^2 + c_2^2 - 4c_3} \tag{9}$$

Whereas equation (9) relates the induced ROC to normal displacements on the structural panel, another equation can be derived that relates the ROC to tile size (or span) requirements and the magnitude of a maximum allowable deflection (see fig. 5(b)). For a tile with dimension L_1 and a deflection limit of $w_{TPS,1}$, an expression for the ROC is

$$\left(\mathrm{ROC} - w_{TPS,1}\right)^2 + L_1^2 = \mathrm{ROC}^2 \tag{10}$$

This expression can be expanded and when solved for ROC yields

$$\mathrm{ROC} = \frac{1}{2}\left(w_{TPS,1} + \frac{L_1^2}{w_{TPS,1}}\right) \tag{11}$$

Results and Discussion

Sandwich Panels

One of the design parameters that must be specified when sizing sandwich panels with the equations in reference 6 is the panel deflection criterion $w_{\max}/d_{HP}$, defined as the ratio of the maximum panel deflection to the panel diameter. In the current study, a panel deflection criterion of 0.01 was chosen to size the sandwich panels. This deflection criterion, together with the material properties and applied pressure loading described previously, resulted in the core and face sheet thicknesses listed in figure 6 for simply supported sandwich panels. For both panel support concepts, the resulting face sheet thickness is the minimum gauge value of 0.04 in.

Linear solutions. The maximum deflections and ROC's for the two hexagonal sandwich panels (support concepts A and D) subjected to a uniform pressure load are listed in table II for simply supported and clamped boundary conditions. For support concept A with simply supported boundary conditions, the maximum deflection of 1.19 in. results in a calculated value of $w_{\max}/d_{HP} = 0.0098$, compared with the design value of 0.01. Since clamping the support points enforces zero slope at those points, the panel maximum displacement is substantially reduced (by 50 percent when the same sandwich design is used). Since the slope is essentially zero at the supports because of symmetry, changing to clamped conditions for panel support concept D has a negligible effect on the maximum panel deflection, as indicated in table II. The maximum deflection yields a calculated value of $w_{\max}/d_{HP} = 0.0090$ for both boundary conditions, which is 10 percent less than the design value.

Nonlinear solutions. Since the maximum panel deflections were on the order of the panel thicknesses for both support concepts A and D, nonlinear finite element analyses were performed to determine the importance of geometric nonlinearities on the predicted performance of the sandwich panels. The results given in table II for support concept A show that small decreases in deflections are predicted by the nonlinear solution, compared with the linear solution. The small decreases in deflections indicate that very little structural stiffening is being induced by the membrane stresses. A slightly larger nonlinear effect is noted for the panel with support concept D, however, because the ratio of the plate thickness to the plate diameter is smaller for support concept D than support concept A.

The local ROC was also calculated (with eq. (9)) from the nonlinear displacements for the panels with support concepts A and D. For support concept A with simple supports, the minimum ROC is 618 in., and when the supports are clamped, the minimum ROC increases to 848 in. For support concept D, the type of boundary conditions (simply supported versus clamped) has very little effect on the mini-

mum ROC, and the resulting value is approximately 390 in. for both cases.

Panel coefficient. When the equations in reference 6 are used to size a sandwich panel, the value of panel coefficient α must be specified. The panel coefficient, which accounts for the shape of the panel planform and the location and type of panel supports, is calculated with the results from a finite element analysis. The coefficient is defined by equation (18) in reference 6 and is

$$w_{\max} = \alpha \frac{p\, d_{HP}^4}{D_{HP}} \tag{12}$$

where $w_{\max}$ is the maximum normal deflection. Panel coefficient values were calculated for support concepts A and D with both the linear and the nonlinear results obtained in this study and are listed in table II. The linear and nonlinear values of α given in table II for panel support concept A with simply supported boundary conditions agree very closely. However, if clamped conditions are assumed for support concept A, the value of α used to size a sandwich panel should be between 0.00389 and 0.00395, as shown in table II. This would lead to a thinner and lighter weight panel design. The panel coefficient does not vary significantly (from 0.00100 to 0.00106) when the boundary conditions are changed from simply supported to clamped for support concept D.

Panel mass. The equations ((23) and (24) from ref. 6) for determining the core and face sheet thicknesses for a minimum mass sandwich panel are, respectively,

$$t_{c,mm} = \left[8\alpha \frac{\rho_f}{\rho_c} \frac{\left(1-\nu_f^2\right)}{E_f} \frac{p\, d_{HP}^3}{(w_{\max}/d_{HP})} \right]^{1/3} \tag{13}$$

$$t_{f,mm} = 0.25 \frac{\rho_c}{\rho_f} t_{c,mm} \tag{14}$$

Using these equations to size the sandwich panels results in minimum mass designs for both support concepts A and D with face sheets thinner than the minimum gauge thickness assumed in this study. For support concept A, the minimum mass design has a face sheet thickness of 0.0229 in., and for support concept D the minimum mass face sheet thickness is 0.0152 in. The consequence of assuming a minimum face sheet thickness greater than the thickness associated with the minimum mass design (as done in the current study) is given in figure 8. In this figure, the variation in the percentage of mass increase over the minimum mass design is shown as a function of the face sheet thickness. Assuming a minimum thickness of 0.04 in. results in a sandwich design that is 30 percent heavier than the minimum mass design for support concept D, and 9 percent heavier for support concept A.

Isogrid Panels

Because the clamped boundary conditions improved the performance for support concept A (but had no effect on support concept D), only clamped supports were studied for the isogrid panels. The panels were designed according to equation (2), with the total isogrid panel mass M_{IP} set equal to the appropriate total sandwich panel mass value listed in figure 6 for each of the two support concepts. In the following results, three normal panel deflections will be discussed: deflections along the ribs, the absolute deflection of the center of the skin in the triangular cells; and the skin-center relative deflection, which is the deflection of the center of the skin relative to the plane formed by the ribs that make up the sides of the triangular cell. Also, to calculate values of ROC, two sets of deflections are considered (as shown in fig. 9(a)): deflections from the interior of a triangular cell (skin) over a rib to the interior of an adjacent triangular cell (skin-rib-skin), and skin deflections that include the center of the triangular cell (skin-center).

Linear solutions. The change in transverse panel displacements (normalized to the panel diameter) as a function of varying skin thickness is shown for a panel with support concept A and rib frequency $F = 1$ in figure 10. Since the amount of mass is held constant for the designs shown in figure 10, as the skin thickness is increased, the amount of material available for the ribs is decreased, resulting in the deflection trends shown in the figure. The design with the smallest value of skin thickness (0.08 in.) has very large absolute and relative skin deflections, but small deflections along the ribs. As the skin thickness is increased, the skin deflections also decrease; however, the deflections along the ribs increase because mass is being taken from the ribs and put into the skin. As even more material is added to the skin, the ribs have so little material that their stiffness is no longer significant and the panel behavior begins approaching that of a very thin uniform plate, and the deflections become very large again. Thus, there are two distinct regions present in the displacement curves given in figure 10: region A, where the lack of skin stiffness dominates the resulting deflections, and region B, where the lack of rib stiffness dominates the deflections. Consequently, there is a most efficient distribution of panel mass between the skin

and the ribs that results in the best isogrid panel performance (smallest maximum deflection).

One finding from the linear results is that the predicted relative skin deflections are very large compared with the skin thickness, varying from a ratio of 35.4 to 7.1 for skin thicknesses of 0.08 and 0.13 in., respectively. Thus, a nonlinear analysis must be performed to obtain accurate displacement information for the isogrid panels.

Another finding is that compressive membrane stresses develop in the thin skins of the triangular cells during panel deformation, and thus skin buckling between the ribs is possible and must be considered in the panel design. Physically, the total skin loading due to the normal pressure loading on the panel can be thought of as caused by two deflection components (see fig. 9). First, when the pressure is applied, the skin deflects laterally as shown in figure 9(a). If the triangular cell is assumed to be clamped at its boundary (as represented by stiff ribs), the large (i.e., greater than the skin thickness) normal deflection causes tensile membrane stresses in the skin because the skins are so thin that membrane action is dominant and very little bending takes place. Second, the skins are attached to the tops of the ribs, and since the neutral axis for panel bending is close to the neutral axis of the ribs (see fig. 7), the pressure causes the ribs to bend as shown in figure 9(b). For the rib deflections shown (which would occur in the center of a panel with support concept A, for example) the size of the triangular cell formed by the tops of the ribs in the deformed structure will be smaller than the initial undeformed size. Thus, the action of the ribs in this case would be to reduce the size of the triangular skin attached to the tops of the ribs (shown by the cross-hatched area in fig. 9(b)) and thereby induce compressive stresses in the skin. Whether the net stress in the skin from these two deflection components is tensile or compressive will depend on the relative stiffnesses of the skin and the ribs.

Isogrid panel buckling design. Since compressive stresses occur in the skins of the isogrid panels, buckling must be considered in their design. When nonlinear analyses were performed, some isogrid designs having low skin stiffness exhibited a bifurcation point before the full design load was reached. (A bifurcation point is indicated with this nonlinear analysis when, as the load is increased incrementally, a negative diagonal term occurs in the total stiffness matrix.) This bifurcation point indicated that a secondary equilibrium path existed for the isogrid skins (see ref. 14). In order to determine the buckling modes for the isogrid panel, a linear bifurcation buckling analysis was run for an isogrid panel with support concept A and $F = 1$.

In the first mode obtained from the linear bifurcation buckling analysis, the skin in a triangular cell section deforms into a half wave with the maximum deflection in the center of the skin (figs. 11(a) and 11(b)). The first six buckling modes of this panel involve each of the six triangular cells successively buckling at essentially identical critical loads. This first mode is identical to the skin deformation shape that results from the transverse pressure loading. Thus, this first mode does not manifest itself in the nonlinear analysis as a bifurcation point (see ref. 15). The bifurcation buckling analysis also identified a second buckling mode that involves skin buckling into a full wave across triangular cells, as illustrated in figures 11(c) and 11(d). It is this bifurcation point that is identified by the nonlinear analysis, and this mode can be thought of as a bifurcation point from a nonlinear prebuckling deformation state. Since the prebuckling deformations are in fact nonlinear, the critical load predicted by the linear bifurcation buckling analysis will not be accurate, and thus the analysis cannot be used for design purposes.

In this study, acceptable isogrid panel designs for support concepts A and D are defined to be those in which the design load was less than the bifurcation load. The reason for this criterion is that at this bifurcation load, the panel would have to change its deformation state drastically from a prebuckling shape that looks identical to the mode in figures 11(a) and 11(b) to the postbuckling shape given in figures 11(c) and 11(d). If this involved very large changes in deflections, or occurred rapidly, the results could be catastrophic for the panel. The nonlinear analysis was used to predict this bifurcation point and eliminate unacceptable designs (i.e., those with insufficient skin thickness).

Nonlinear solutions. Isogrid panel designs that did not buckle under the design pressure, along with their maximum deflections, are tabulated in tables III and IV for support concepts A and D, respectively. In both cases, increasing the rib frequency F decreases the length of the triangular cell sides L_{tcs}, which leads to thinner skins in the acceptable designs. In general, for a given rib frequency, the design that has the minimum skin thickness to prevent skin buckling, and thus the greatest amount of material in the ribs, gives the best (i.e., smallest) deflection performance for both support concepts.

Tables III and IV also show that for a given rib frequency, acceptable isogrid panel designs with support concept D have skin thicknesses smaller than

those for support concept A. This occurs because the magnitudes of the compressive membrane stresses (N_R and N_θ) for support concept D (see fig. 12) are significantly smaller than the stresses for concept A (see fig. 13). Thus, skin thicknesses required to resist buckling are smaller for support concept D. The results in figures 12 and 13 also show that support concept A has a much larger portion of the skin surface in a compressive stress state than does support concept D. Representative deflection shapes are shown for the same isogrid panels with $F = 3$ and support concepts A and D in figures 14 and 15, respectively. The relative skin deflections are much more pronounced in support concept D because acceptable designs had thinner skins than the designs for concept A. Although these relative skin displacements predicted by the nonlinear analysis are less than those predicted by the linear analysis, they are still large compared with the skin thickness, as shown in figure 16.

The maximum displacements of the best performing panels for the two support concepts are compared in figure 17. For support concept A, the maximum panel displacement predicted by the nonlinear analysis for the best design is 1.11 in. and is associated with an $F = 4$ design. Similarly, for support concept D, the maximum displacement for the best design is 0.75 in. and is associated with an $F = 3$ design. The results in figure 17 show that the maximum displacement for both support concepts is not very sensitive to F (or L_{tcs}) in the vicinity of the best designs, thus giving some flexibility to the panel designer.

The nonlinear deflection performance of equal mass sandwich panels with support concepts A and D is indicated by the horizontal lines in figure 17. For support concept A, the isogrid panel with the best design has a deflection almost twice as large as that of the sandwich panel design. In order to obtain equal performance, the rib thickness for the $F = 4$ design had to be increased from 0.23 in. to 0.28 in. As a result, the equal performance isogrid panel became 26 percent heavier than the sandwich panel. For support concept D, the isogrid panel design with $F = 3$ has a maximum deflection that is only 57 percent of the sandwich panel deflection. An equal performance design for an isogrid panel with support concept D, having a skin thickness of 0.07 in. and a rib thickness of 0.28 in., has a mass that is 7 percent less than the sandwich panel mass.

The relationship between the radius of curvature and the allowable TPS tile size and deflection (as given in eq. (11)) is illustrated in figure 18. The results show that if an allowable TPS deflection is specified, the minimum ROC on the deflected structure increases as the TPS tile size increases. This means that larger TPS tiles would require a stiffer support structure. If the structure has already been designed for minimum mass based on a deflection criterion, the ROC will already be given. In this case, the maximum TPS tile size will be dictated by the maximum allowable deflection, and increasing the deflection limit will allow larger tiles to be used.

Skin-center and skin-rib-skin ROC results for the isogrid panel designs presented in figure 17 are given in table V. Generally, the panels with support concept A have larger ROC's than the panels with support concept D, and thus would place less stringent limitations on the TPS design. For both support concepts, the normal deflections from the thin skins on one side of a rib, over the stiff rib to the thin skin on the other side of the rib, give the smallest ROC. For isogrid designs with performance equal to the corresponding sandwich panels, the panel with support concept A has a minimum ROC of 124 in. and the panel with support concept D has a minimum ROC of 76 in. These values are substantially smaller than the ROC's of 848 in. and 387 in. for the sandwich panels with support concepts A and D, respectively.

Concluding Remarks

Structural sizing and performance data have been presented for two aerobrake hexagonal heat shield panel structural concepts. One concept features a sandwich construction with an aluminum honeycomb core and thin quasi-isotropic graphite-epoxy face sheets. The other concept features a skin-rib isogrid construction with thin quasi-isotropic graphite-epoxy skins and graphite-epoxy ribs oriented at 0°, +60°, and −60° along the panel. Two concepts for attaching the panels to the support truss were evaluated for each of the two panel concepts. Linear static, linear bifurcation buckling, and nonlinear static analyses were performed to compare the structural performance of the two panel concepts and assess their feasibility for a lunar transfer vehicle aerobrake application.

Although clamped supports are difficult to achieve practically, changing the boundary conditions at the panel support points from simply supported to clamped was theoretically effective in reducing the deflections for a panel supported at the three vertices. In this case, changing only the boundary conditions reduced the maximum panel deflection

by 50 percent. However, changing the boundary conditions had no effect on the deflections of the panel with interior supports because the slope at the support points was already essentially zero because of the interior location of the supports.

Geometrically nonlinear effects were found to be small in the sandwich concept, and thus linear analysis could be used to accurately design and assess the panel performance. Efficient isogrid panel designs were found to have very thin skins supported by ribs that can be very widely spaced. Nonlinear analysis predicted that these designs would have skin deflections that were several times the skin thickness. Rib bending induced compressive membrane stresses in large portions of the skins in the isogrid panels. This is because for thin skins, the effective neutral axis of the skin-rib combination was located in the ribs. Because of the large skin deflections and compressive membrane stresses, nonlinear static analyses that can predict skin buckling must be used to determine viable isogrid panel designs and obtain accurate performance data.

The equations for calculating the local panel radius of curvature (ROC) from normal panel displacements were solved symbolically and presented in a useful form for general use. The minimum ROC of the structure supporting the thermal protection system (TPS) was found to be a useful quantity for relating the structural and TPS design requirements. Equations were developed that show a potential relationship between structural and TPS designs. A design chart that relates the ROC of the structure to the TPS tile size and deflection limit has been given and should be useful for designing a heat shield structure based on TPS requirements.

Sandwich and isogrid panels having the same maximum deflection were designed for both support concepts. For the panel with clamped supports at three of the vertices, the sandwich design was found to be superior, since it has only 79 percent of the mass of the corresponding isogrid panel. In addition, the sandwich panel has a minimum ROC much greater than that of the isogrid panel, and thus would place less restrictions on the TPS design. For the panel with three clamped supports in the panel interior, an isogrid panel with equal deflection performance has slightly less (7 percent) mass than the sandwich panel. However, the sandwich mass can be further reduced (by 30 percent) if the minimum gauge assumption of 0.04 in. for the face sheets is relaxed and a minimum mass design is used. Once again, the sandwich panel has the additional advantage of having a minimum ROC much greater than that of the isogrid panel, and from that standpoint, it has the advantage of placing less restrictions on the TPS design.

NASA Langley Research Center
Hampton, VA 23665-5225
March 27, 1992

References

1. *Report of the National Commission on Space: Pioneering the Space Frontier.* Bantam Books, Inc., 1986.

2. Mikulas, Martin M., Jr.; and Dorsey, John T.: *An Integrated In-Space Construction Facility for the 21st Century.* NASA TM-101515, 1988.

3. Walberg, Gerald D.: A Review of Aerobraking for Mars Missions. Paper No. IAF-88-196, Oct. 1988.

4. Braun, Robert D.; and Blersch, Donald J.: Propulsive Options for a Manned Mars Transportation System. AIAA-89-2950, July 1989.

5. Dorsey, John T.; and Mikulas, Martin M., Jr.: *Preliminary Design of a Large Tetrahedral Truss/Hexagonal Heatshield Panel Aerobrake.* NASA TM-101612, 1989.

6. Dorsey, John T.; and Mikulas, Martin M., Jr.: Preliminary Design of a Large Tetrahedral Truss/Hexagonal Panel Aerobrake Structural System. AIAA-90-1050, Apr. 1990.

7. Slysh, Paul: The Isogrid King of Lightweight Design. *Mach. Design*, vol. 45, no. 9, Apr. 19, 1973, pp. 102–107.

8. Abraham, Lewis H.; and Lowy, Mortimer J.: Shell Instability Problems as Related to Design. *Collected Papers on Instability of Shell Structures 1962.* NASA TN D-1510, 1962, pp. 1–9.

9. Sylvester, Richard J.: Stability Problems in Missile Structures. *Collected Papers on Instability of Shell Structures 1962*, NASA TN D-1510, 1962, pp. 11–20.

10. *The Office of Exploration FY 1989 Annual Report Exploration Studies Technical Report. Volume II: Space Transportation Systems.* NASA TM-4170, 1989.

11. Whetstone, W. D.: *EISI-EAL Engineering Analysis Language User Instructions, Version 312.08.* Engineering Information Systems, Aug. 1985.

12. Thomas, George B., Jr.: *Calculus and Analytic Geometry,* Fourth ed. Addison-Wesley Publ. Co., c.1968.

13. *Theorist Reference Manual.* Allan Bonadio Assoc./Prescience Corp., c.1989.

14. Brush, Don O.; and Almroth, Bo O.: *Buckling of Bars, Plates, and Shells.* McGraw-Hill, Inc., c.1975.

15. Bushnell, David: Buckling of Shells–Pitfall for Designers. *A Collection of Technical Papers, Part 1 AIAA/ASME/ASCE/AHS 21st Structures, Structural Dynamics & Materials Conference*, May 1980, pp. 1–56. (Available as AIAA-80-0665.)

Table I. Isogrid Stringer Designs

$[[+45, -45, 0_n]_s;\ n \geq 4]$

n	Total number of plies	Total thickness, in.	E_{eff}, psi
4	12	0.06	28.2×10^6
8	20	.10	33.3
12	28	.14	35.5
16	36	.18	36.7
20	44	.22	37.5
24	52	.26	38.0

Table II. Sandwich Panel Deflections and Radius of Curvatures

Support concept A							
Boundary condition	$w_{\max}$, in.		$w_{\max}/D_{SP}$		α		$\text{ROC}_{\min}$, in.
	Linear	Nonlinear	Linear	Nonlinear	Linear	Nonlinear	Nonlinear
Simply supported	−1.19	−1.19	0.0098	0.0098	0.00746	0.00746	618
Clamped	−0.63	−0.62	0.0052	0.0051	0.00395	0.00389	848
Support concept D							
Boundary condition	$w_{\max}$, in.		$w_{\max}/D_{SP}$		α		$\text{ROC}_{\min}$, in.
	Linear	Nonlinear	Linear	Nonlinear	Linear	Nonlinear	Nonlinear
Simply supported	−1.35	−1.29	0.0090	0.0086	0.00105	0.00100	389
Clamped	−1.36	−1.31	0.0090	0.0087	0.00106	0.00102	387

Table III. Panel Performance Comparison—Support Concept A

[Results from nonlinear analyses]

F	t_{sk}, in.	t_{rib}, in.	$w_{\max}/d_{HP}$
1	0.12	0.24	0.0118
1	.13	.19	.0139
2	.10	.24	.0105
3	.08	.24	.0094
3	.09	.22	.0109
4	.07	.23	.0092
4	.08	.21	.0109
5	.06	.22	.0096
Sandwich			.0051
*4	.07	.28	.0050

*Designed for equal performance (w/d_{HP}) of sandwich panel.

Table IV. Panel Performance Comparison —Support Concept D

[Results from nonlinear analyses]

F	t_{sk}, in.	t_{rib}, in.	w_{max}/d_{HP}
2	0.06	0.29	0.0054
2	.07	.26	.0067
3	.04	.29	.0050
3	.05	.27	.0056
4	.04	.25	.0057
4	.05	.23	.0069
Sandwich			.0087
*3	.06	.23	.0084

*Designed for equal performance (w/d_{HP}) of sandwich panel.

Table V. Minimum Radius of Curvatures for Isogrid Panels

[Clamped boundary conditions]

Support concept	F	t_{sk}, in.	t_{rib}, in.	ROC_{min}, in.	
				Skin-center	Skin-rib-skin
A	1	0.12	0.24	402	156
↓	2	.10	.24	163	135
	3	.08	.24	125	100
	4	.07	.23	124	107
	*4	.07	.28	168	124
	5	.06	.22	113	99
D	2	.06	.29	201	83
↓	3	.04	.29	151	54
	*3	.06	.23	134	76
	4	.04	.25	99	49

*Designed for equal performance (w/d_{HP}) of sandwich panel.

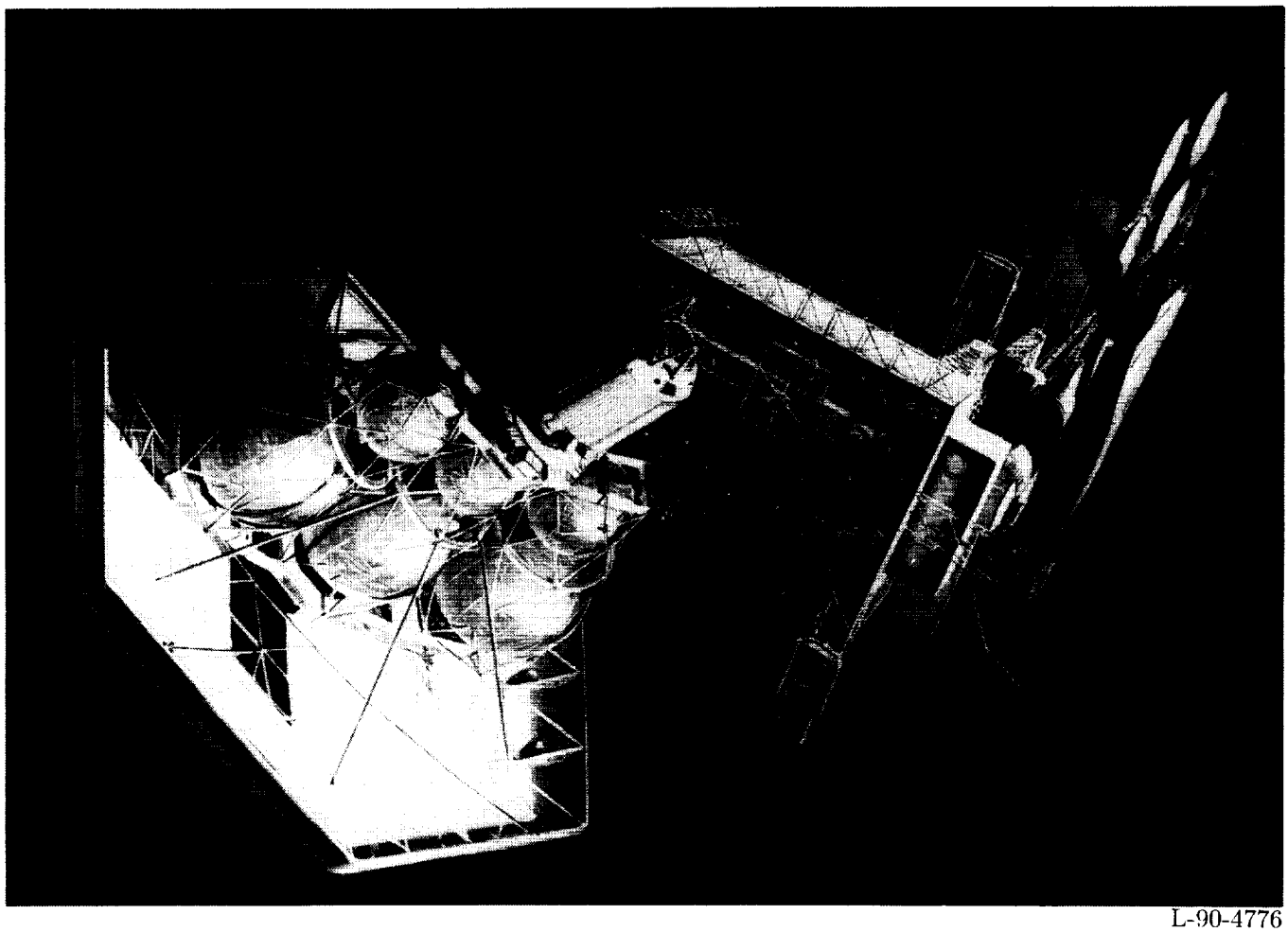

L-90-4776

Figure 1. Orbital transfer vehicle with aerobrake.

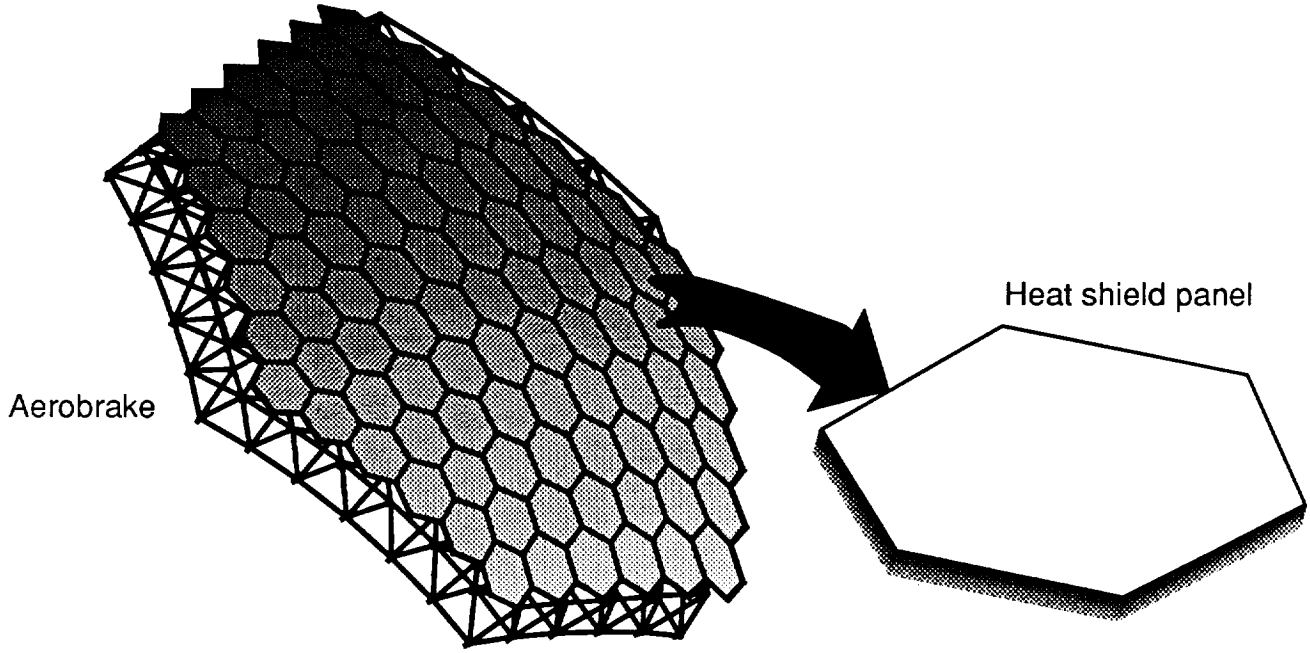

(a) Hexagonal heat shield panels.

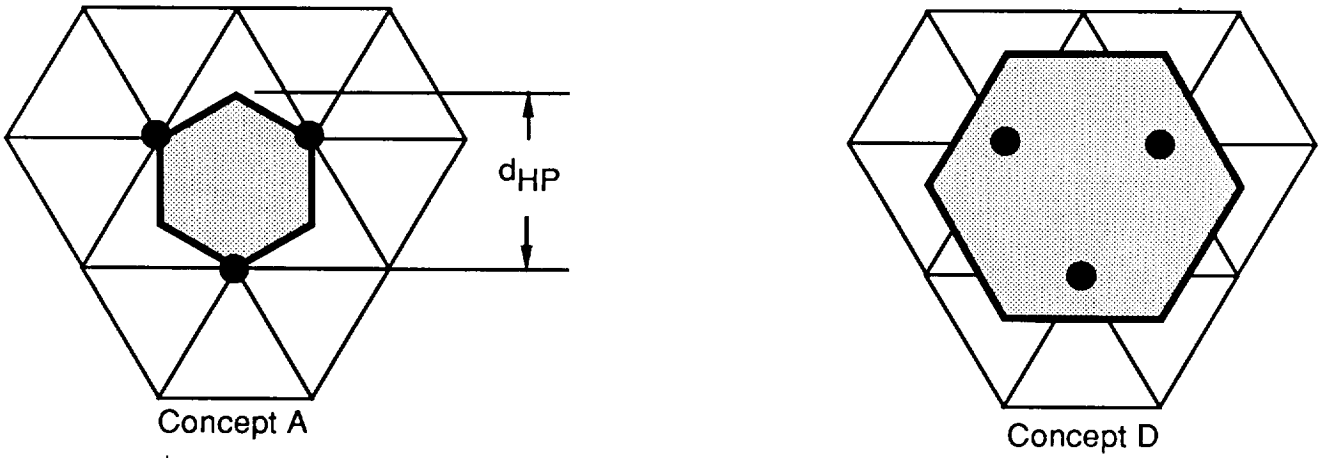

(b) Panel support concepts studied.

Figure 2. Aerobrake and panel support concepts.

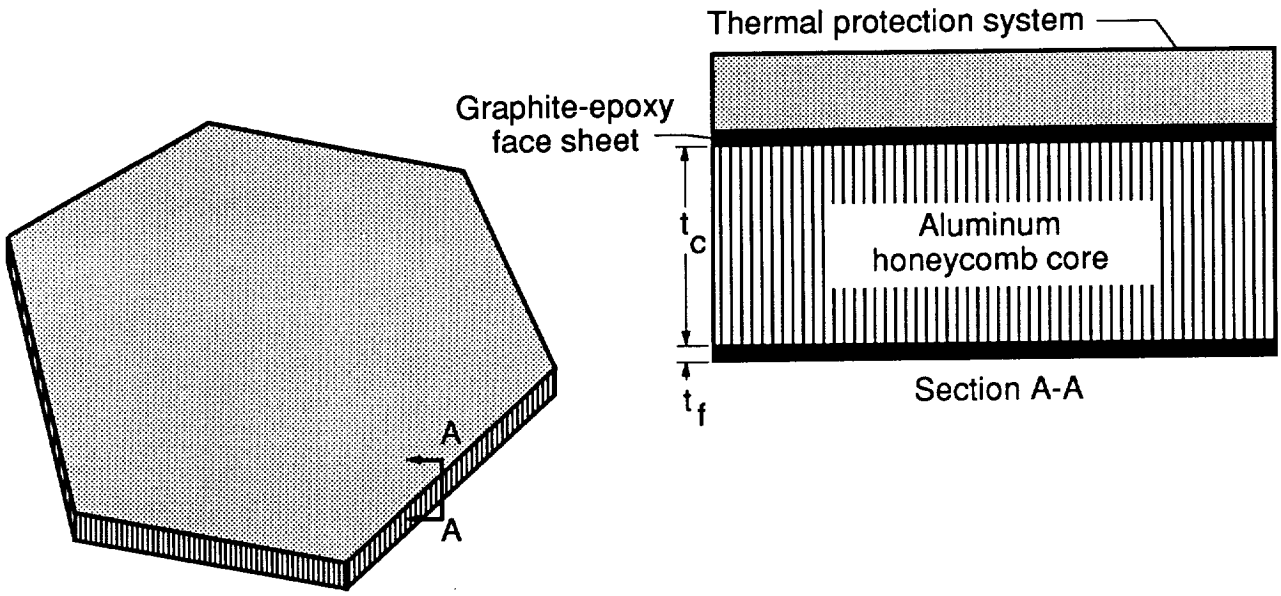

Figure 3. Sandwich panel structural concept.

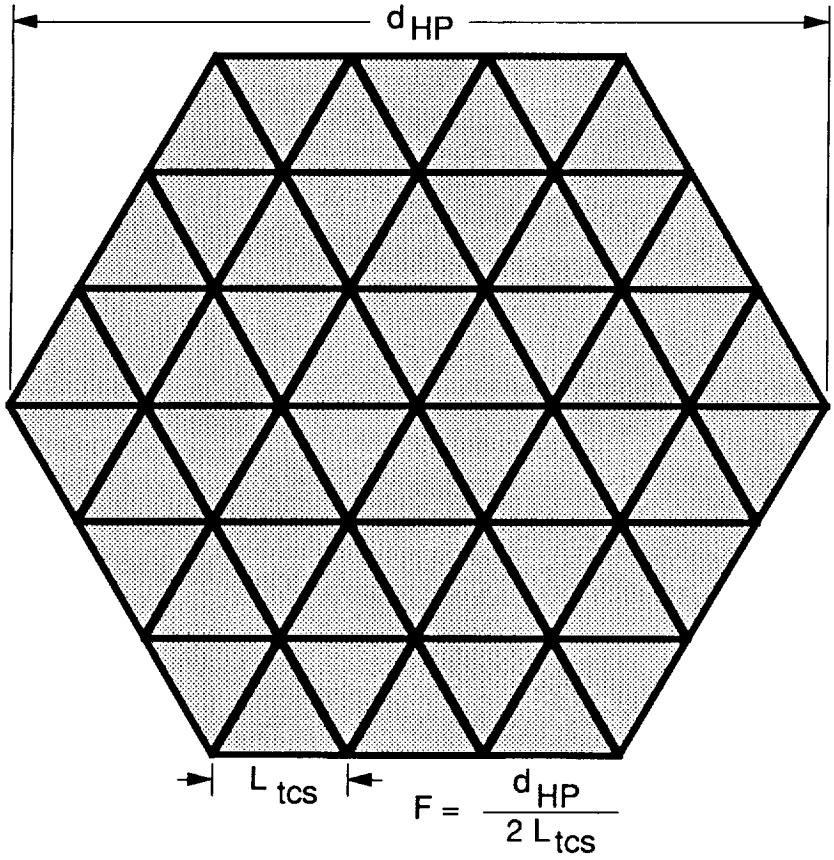

(a) Stringer frequency definition.

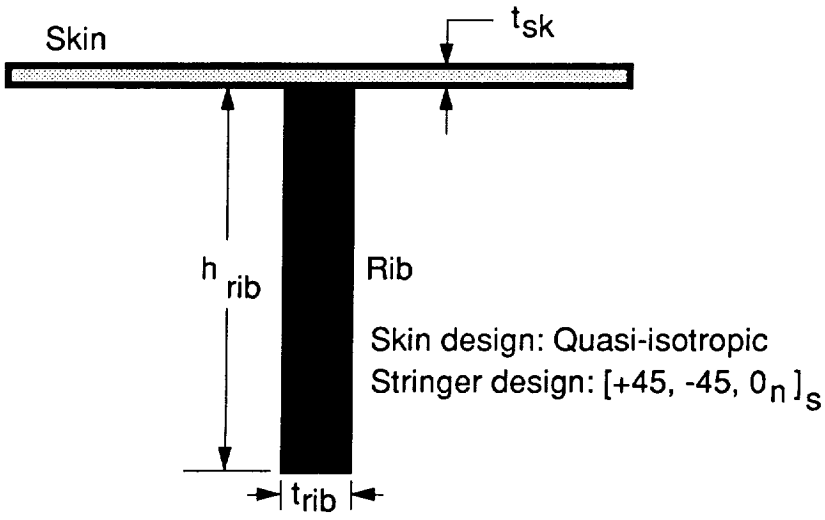

(b) Skin and stringer details.

Figure 4. Isogrid panel structural concept.

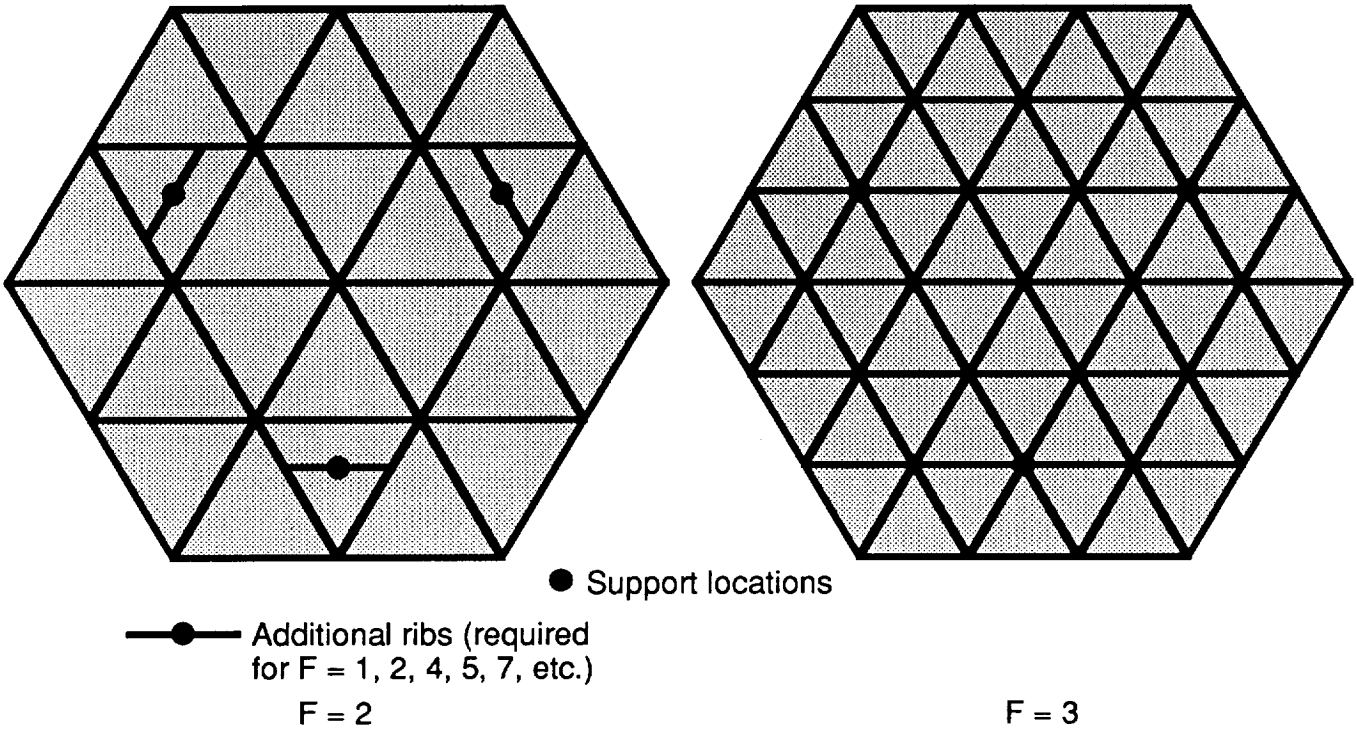

(c) Additional ribs required for support concept D.

Figure 4. Concluded.

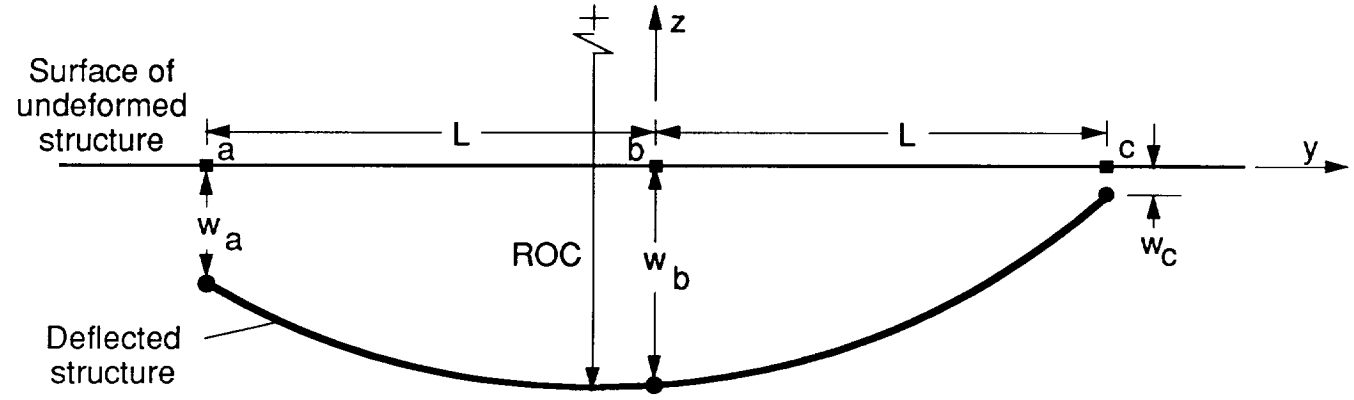

(a) Geometry for calculating ROC from three normal displacements.

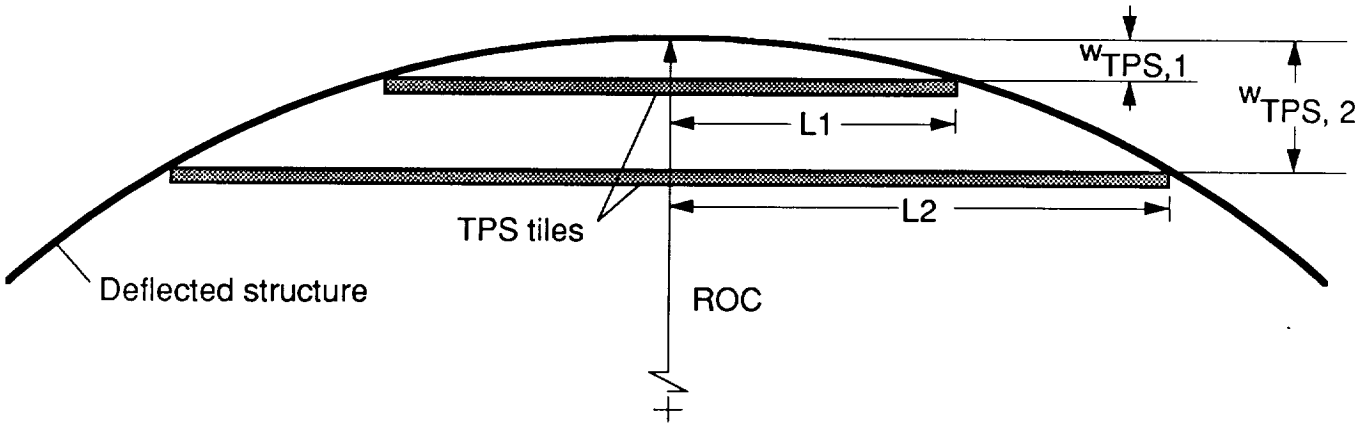

(b) Relationship between TPS panel size, deflection limit, and ROC.

Figure 5. Relationship between TPS tile requirements and structural deflections.

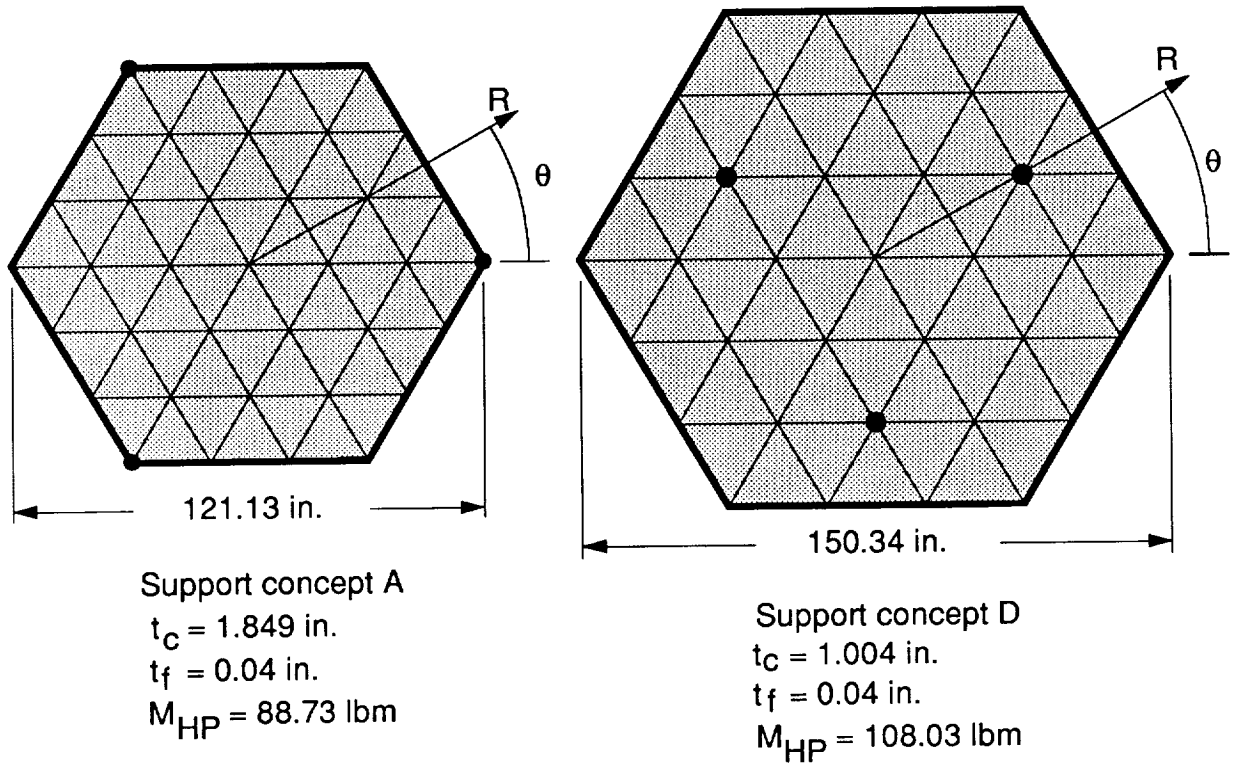

Figure 6. Sandwich panel analysis model.

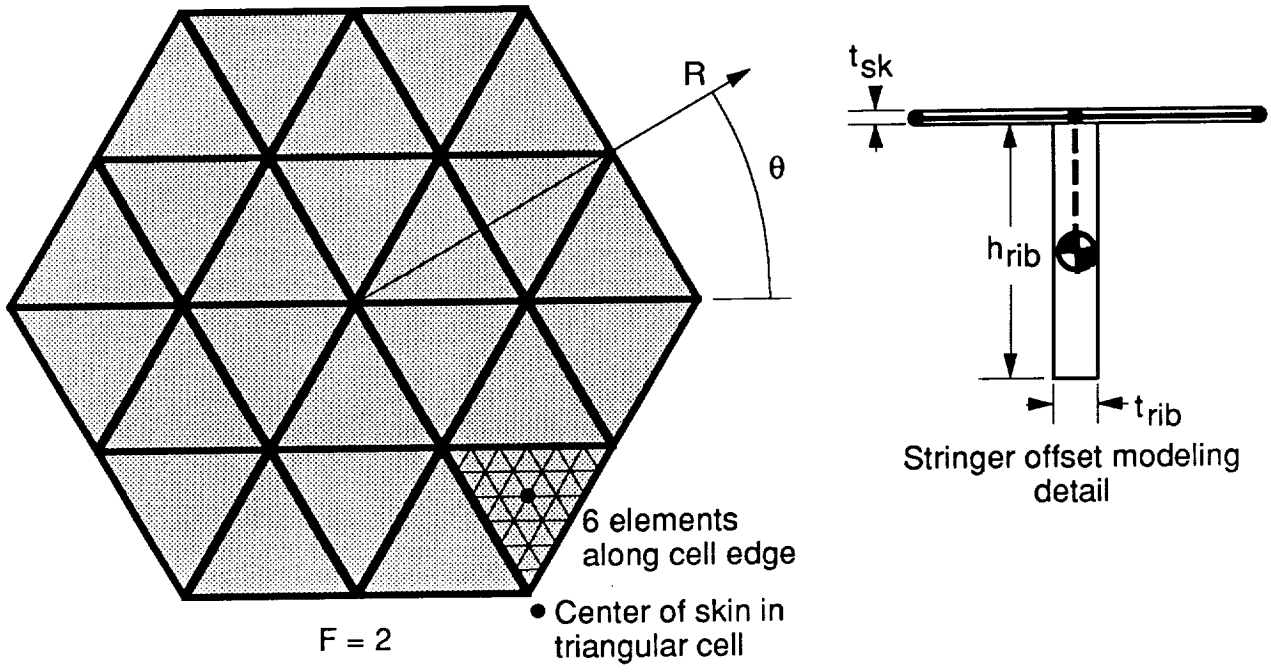

Figure 7. Isogrid panel analysis model.

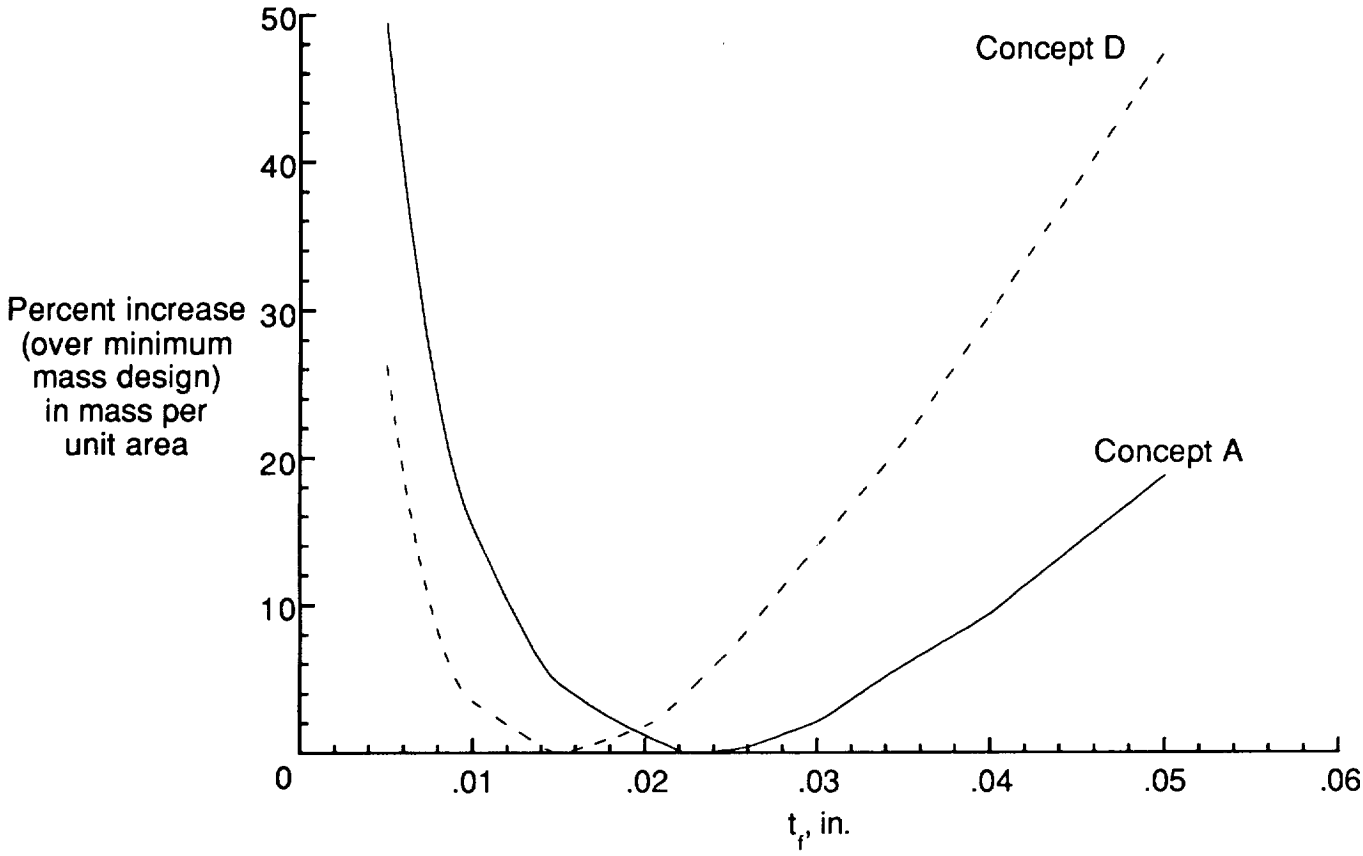

Figure 8. Effect of sandwich face sheet minimum gauge assumption on sandwich panel mass.

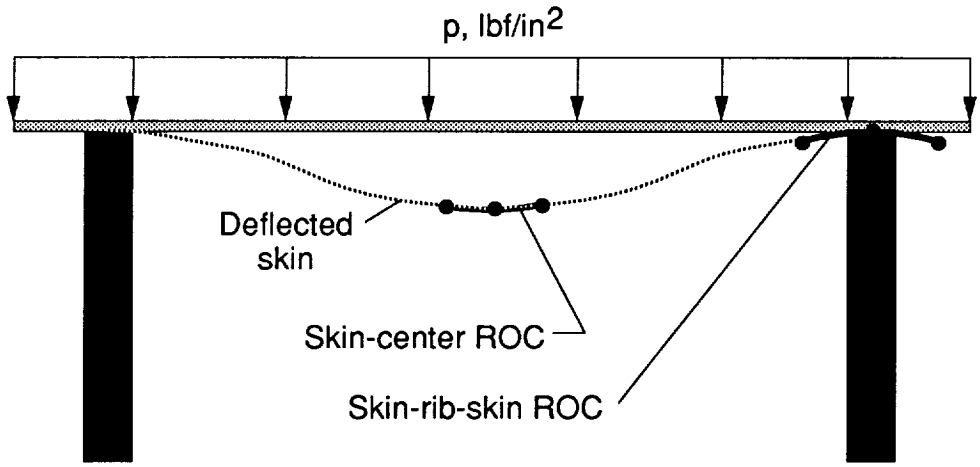

(a) Relative skin deflection.

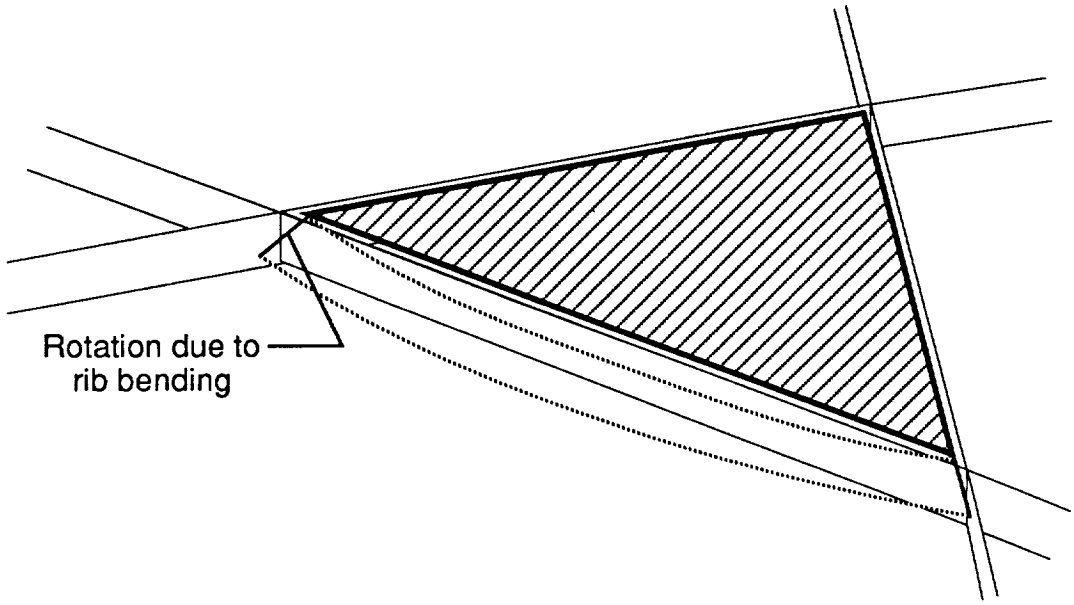

(b) Rib bending deflections.

Figure 9. Skin loading components and ROC definition.

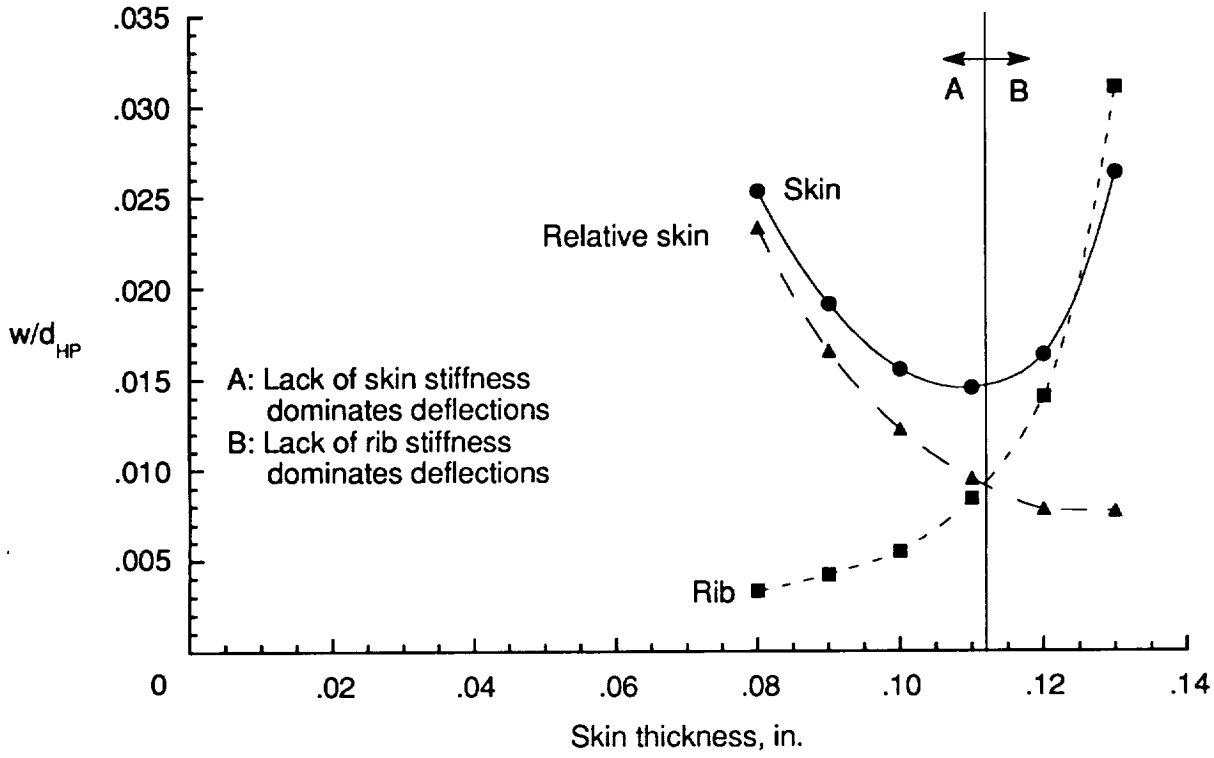

Figure 10. Effect of skin thickness on displacements. $F = 1$; support concept A; linear analysis: clamped.

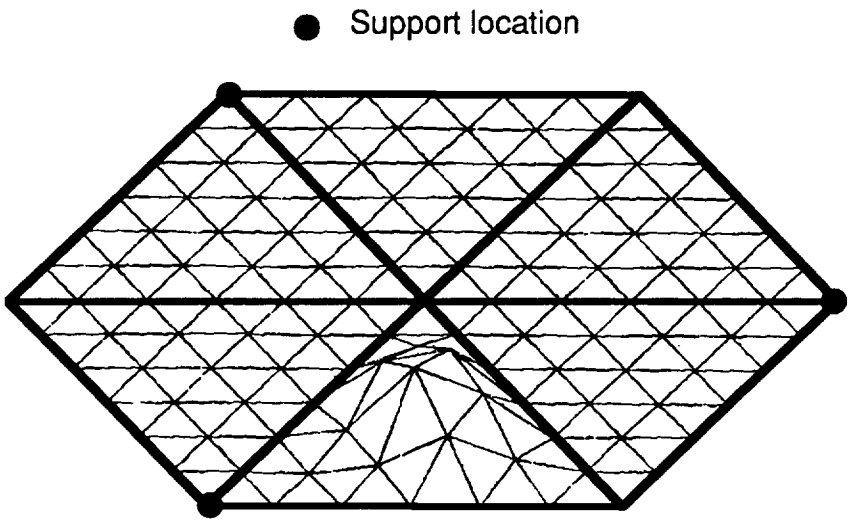

(a) Deflection shape for $N = 1$ mode.

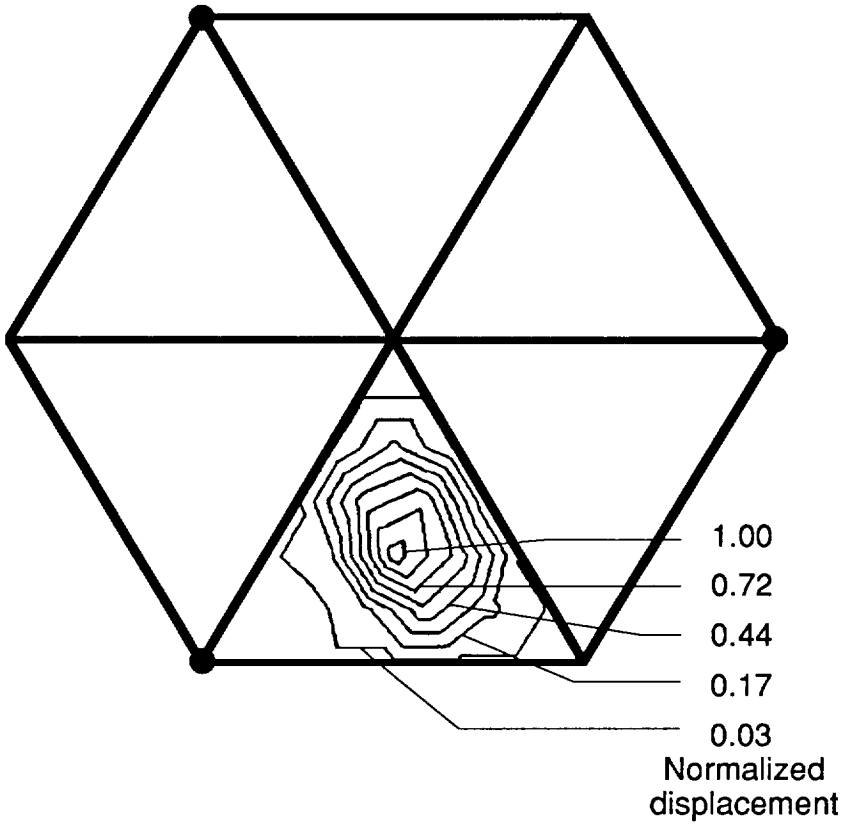

(b) Displacement contour for $N = 1$ mode.

Figure 11. Bifurcation buckling modes predicted for isogrid panel. $F = 1$; support concept A.

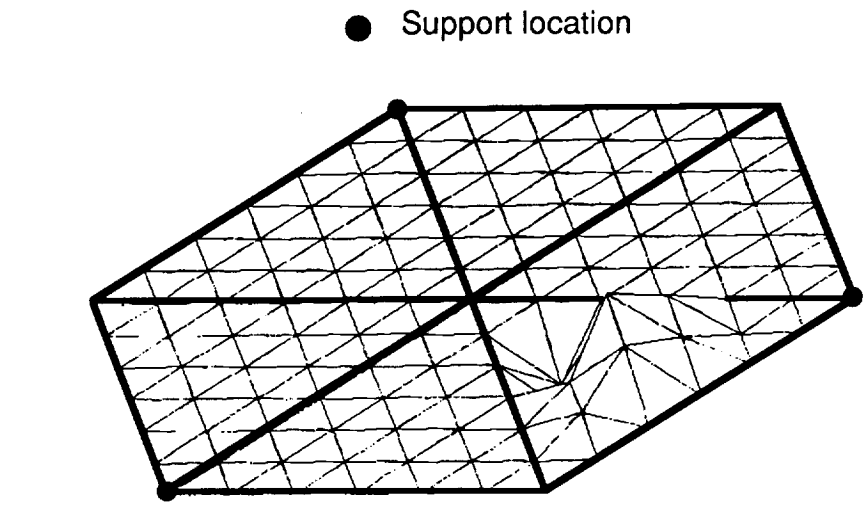

(c) Deflection shape for $N = 2$ mode.

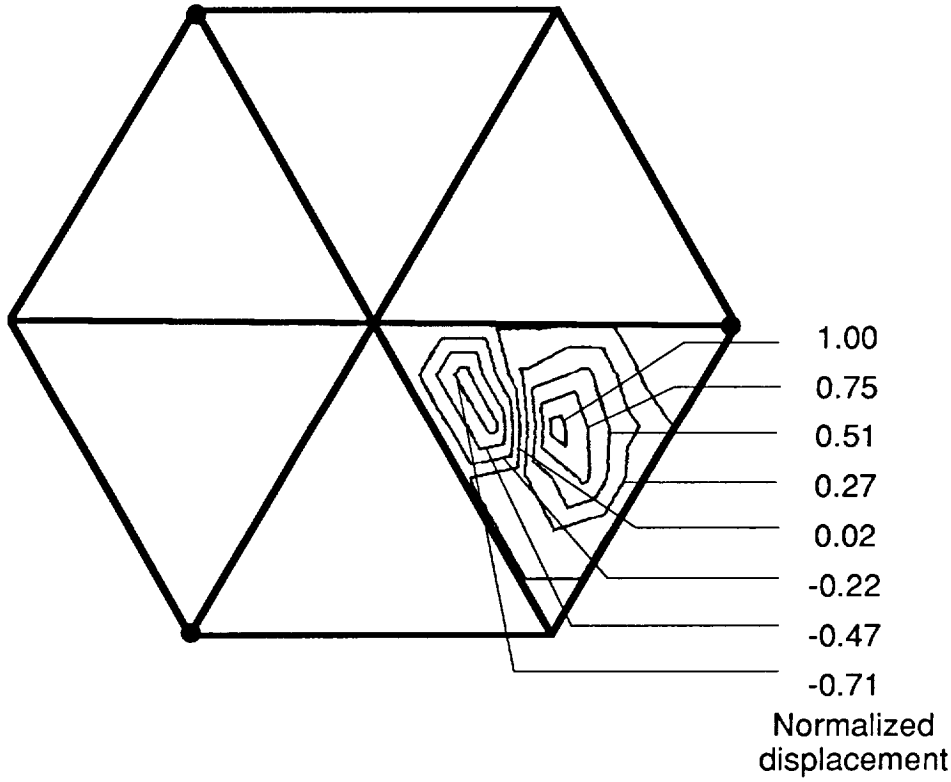

(d) Displacement contour for $N = 2$ mode.

Figure 11. Concluded.

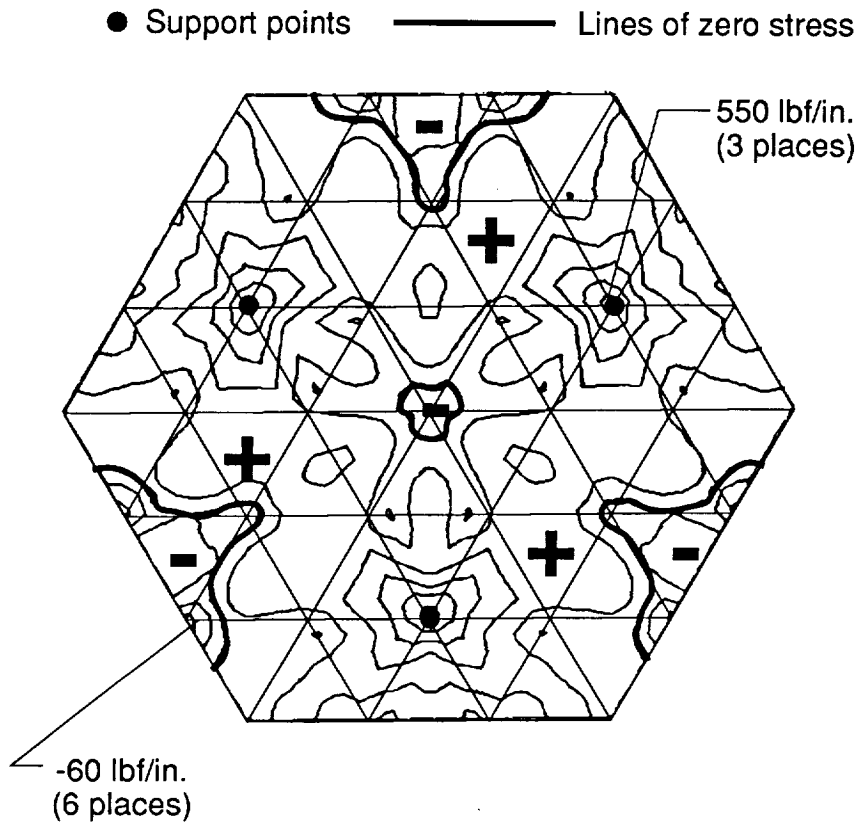

(a) N_R.

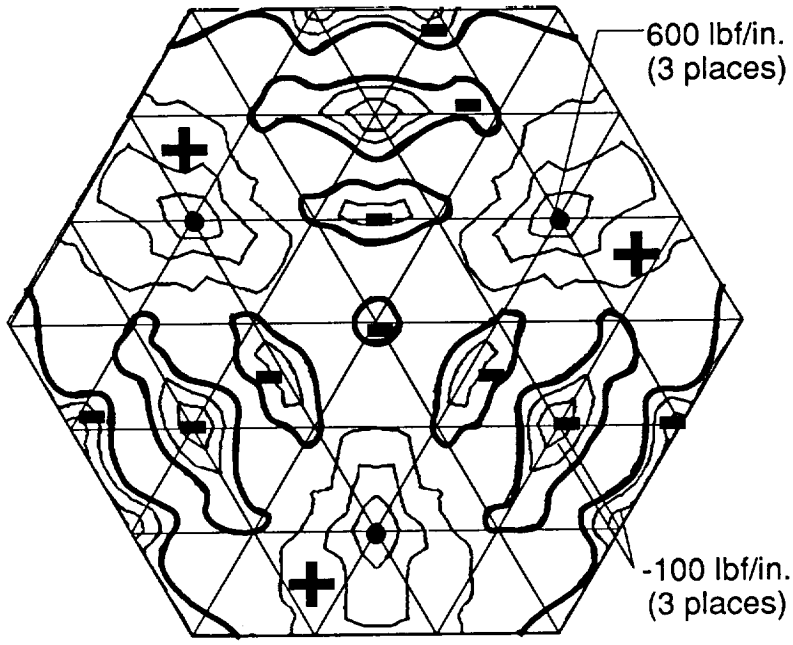

(b) N_θ.

Figure 12. Membrane stress resultants in isogrid skin for support concept D. $F = 3$; nonlinear results.

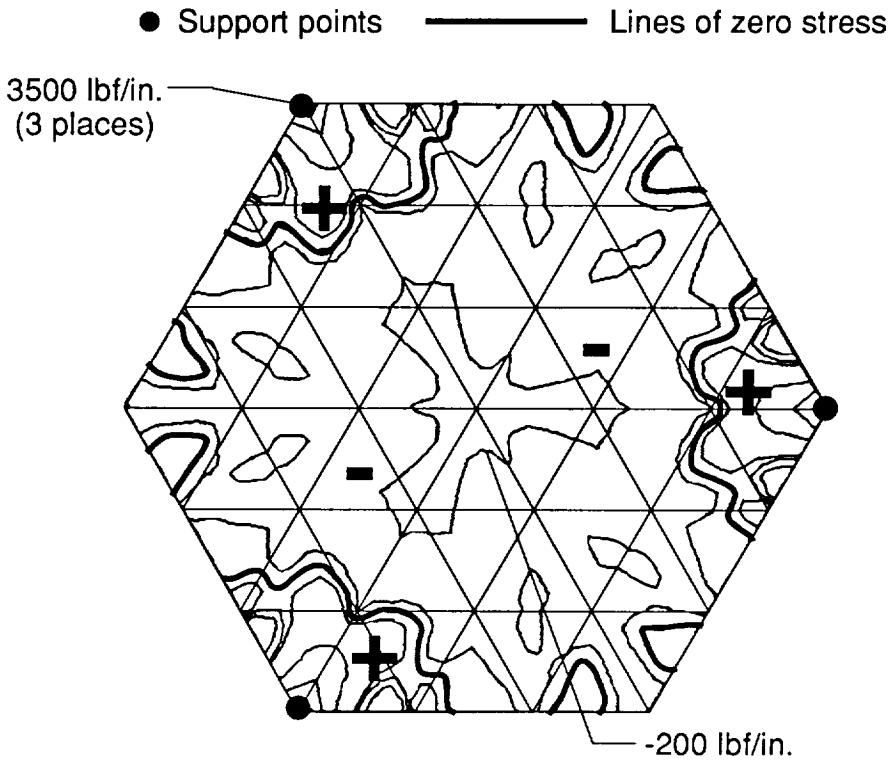

(a) N_R.

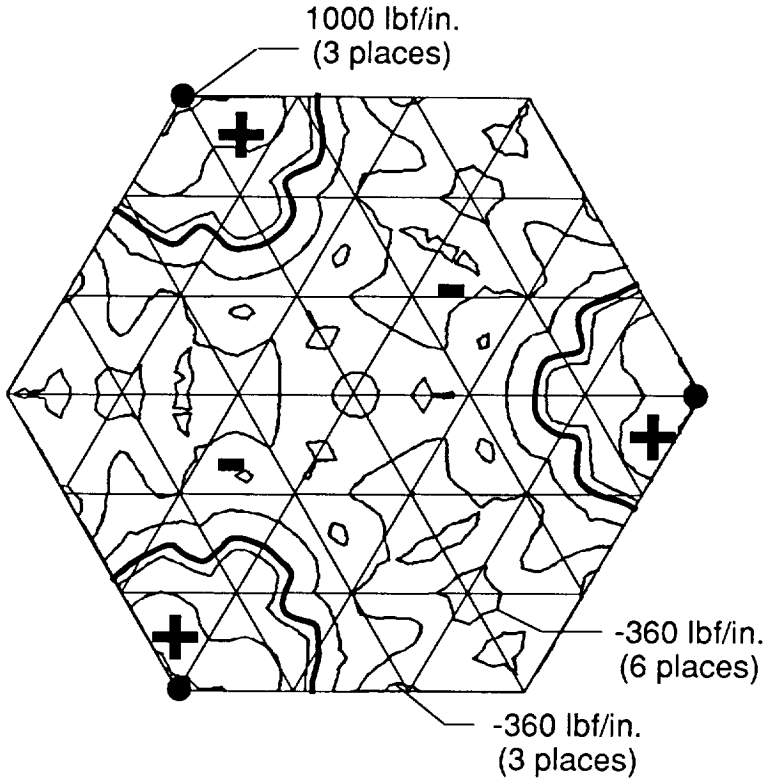

(b) N_θ.

Figure 13. Membrane stress resultants in isogrid skin for support concept A. $F = 3$; nonlinear results.

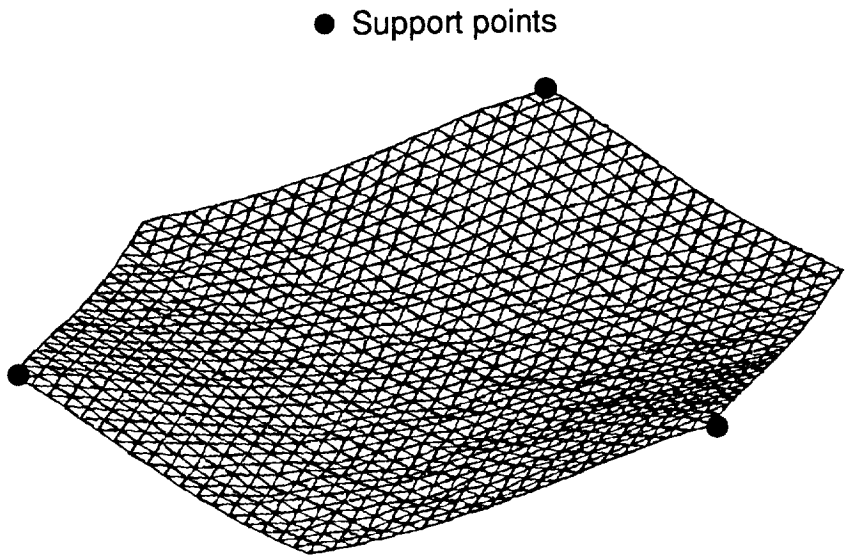

(a) Deflected shape.

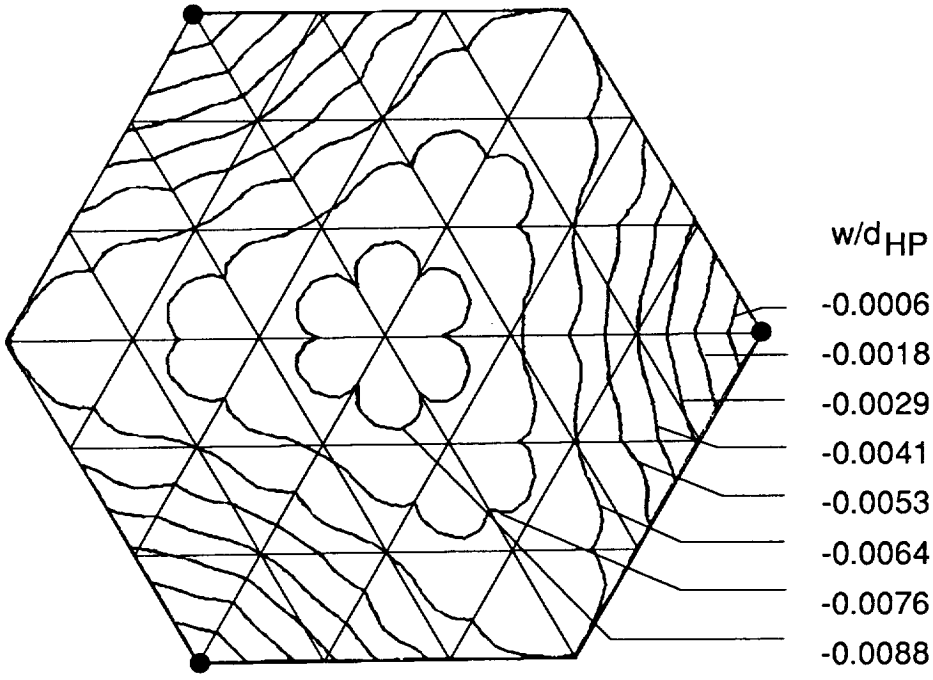

(b) Normal displacement contours.

Figure 14. Representative isogrid displacements for support concept A. $F = 3$; nonlinear results.

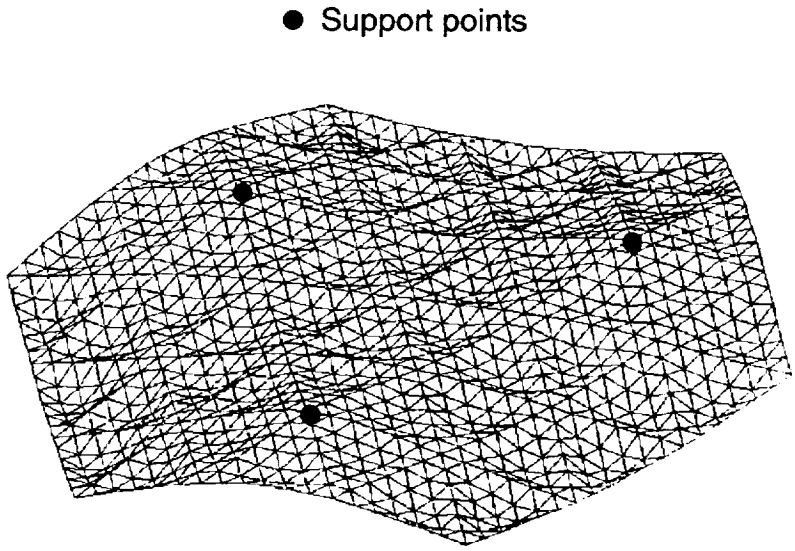

(a) Deflected shape.

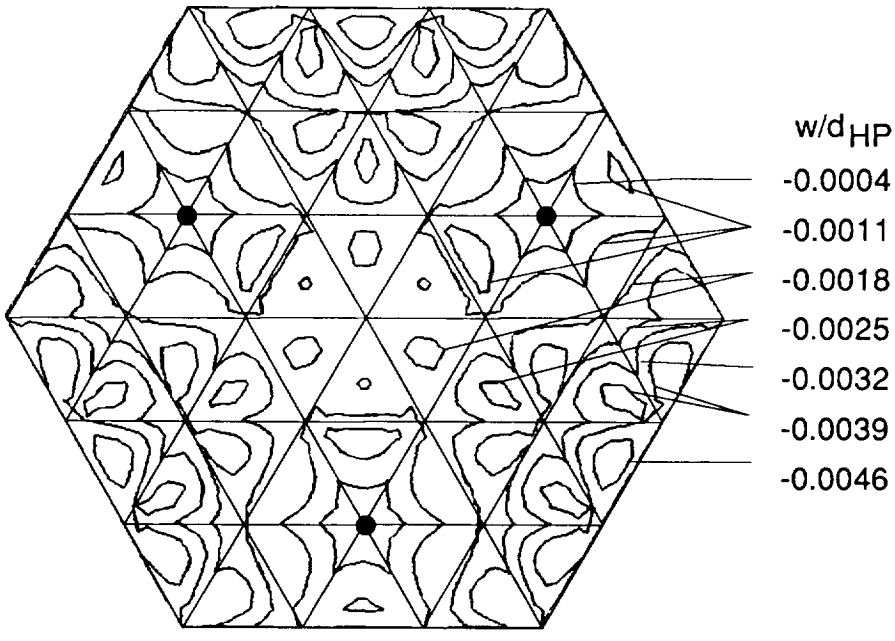

(b) Normal displacement contours.

Figure 15. Representative isogrid displacements for support concept D. $F = 3$; nonlinear results.

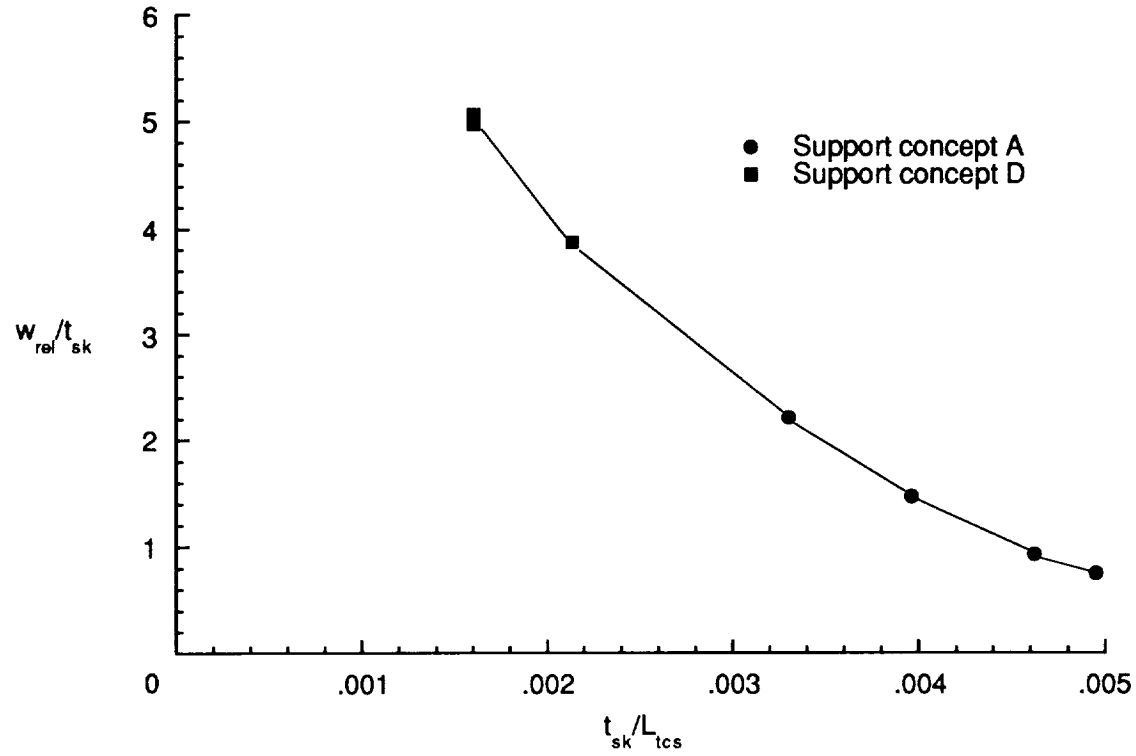

Figure 16. Maximum relative skin deflections (nonlinear analysis).

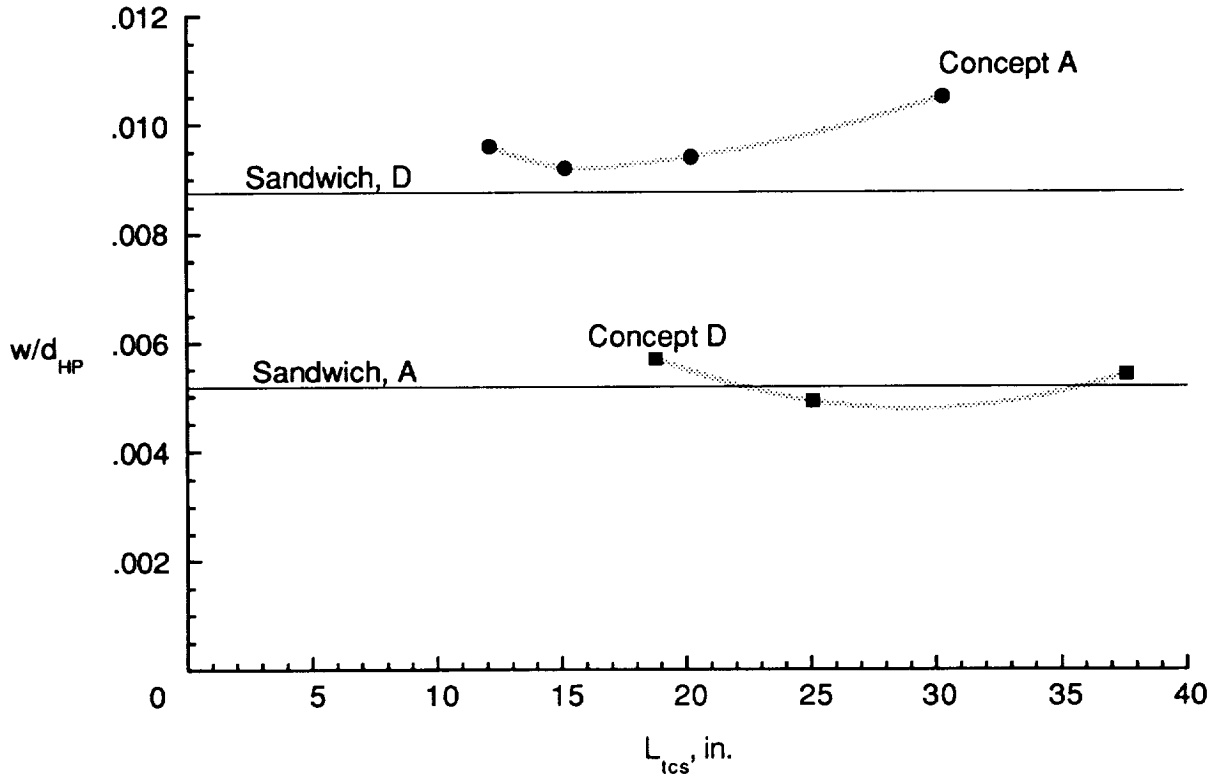

Figure 17. Effect of rib spacing on maximum displacements (nonlinear results).

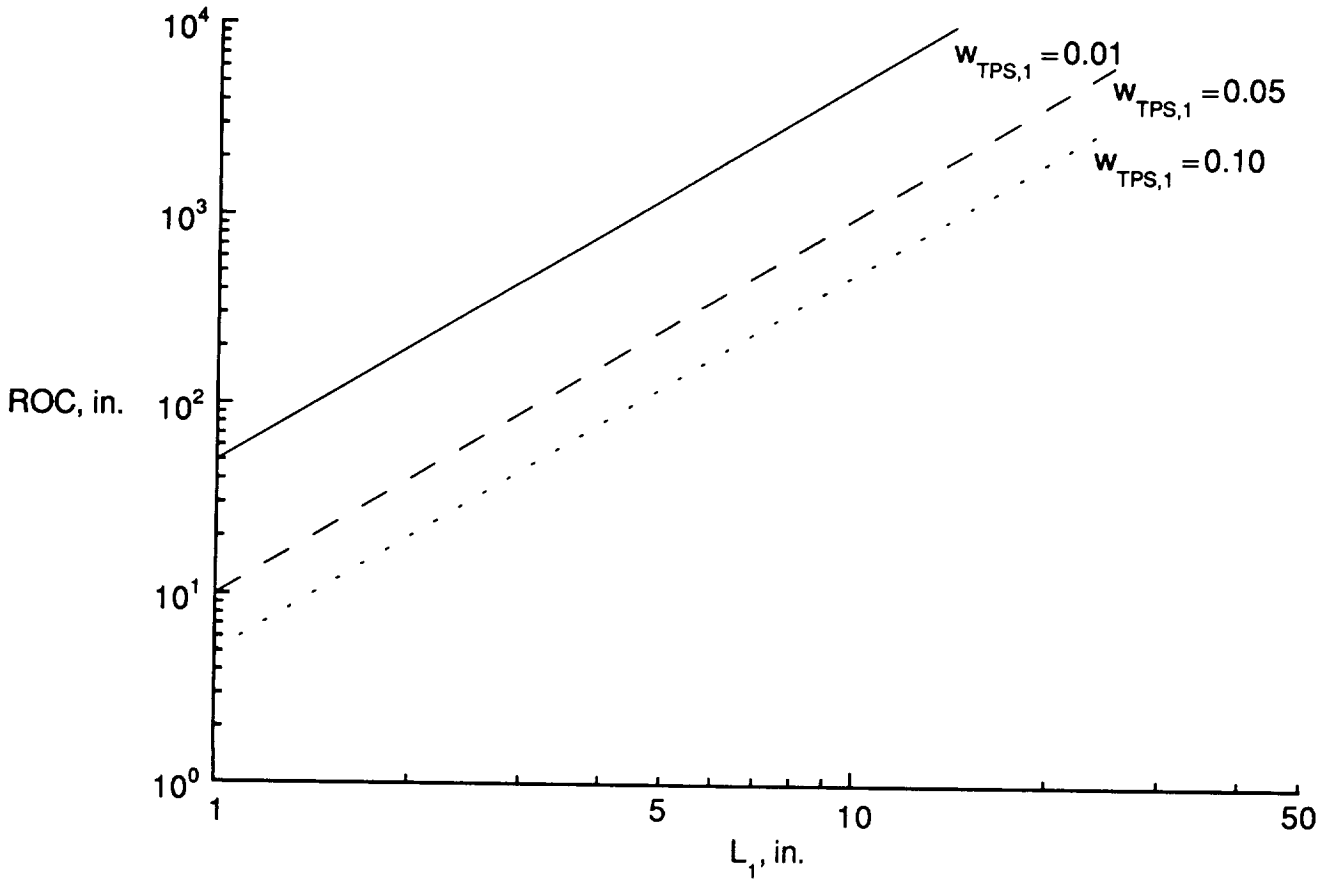

Figure 18. Influence of TPS tile size and allowable deflection on ROC.

REPORT DOCUMENTATION PAGE

Form Approved
OMB No. 0704-0188

1. AGENCY USE ONLY *(Leave blank)*	2. REPORT DATE	3. REPORT TYPE AND DATES COVERED
	May 1992	Technical Memorandum

4. TITLE AND SUBTITLE
Structural Performance of Two Aerobrake Hexagonal Heat Shield Panel Concepts

5. FUNDING NUMBERS
WU 506-43-41-02

6. AUTHOR(S)
John T. Dorsey and James W. Dyess

7. PERFORMING ORGANIZATION NAME(S) AND ADDRESS(ES)
NASA Langley Research Center
Hampton, VA 23665-5225

8. PERFORMING ORGANIZATION REPORT NUMBER
L-17056

9. SPONSORING/MONITORING AGENCY NAME(S) AND ADDRESS(ES)
National Aeronautics and Space Administration
Washington, DC 20546-0001

10. SPONSORING/MONITORING AGENCY REPORT NUMBER
NASA TM-4372

11. SUPPLEMENTARY NOTES
Dorsey: Langley Research Center, Hampton, VA; Dyess: Virginia Polytechnic Institute and State University, Blacksburg, VA.

12a. DISTRIBUTION/AVAILABILITY STATEMENT
Unclassified Unlimited

Subject Category 18

12b. DISTRIBUTION CODE

13. ABSTRACT *(Maximum 200 words)*
Structural sizing and performance are presented for two structural concepts for an aerobrake hexagonal heat shield panel. One concept features a sandwich construction with an aluminum honeycomb core and thin quasi-isotropic graphite-epoxy face sheets. The other concept features a skin-rib isogrid construction with thin quasi-isotropic graphite-epoxy skins and graphite-epoxy ribs oriented at $0°$, $+60°$, and $-60°$ along the panel. Linear static, linear bifurcation buckling, and nonlinear static analyses were performed to compare the structural performance of the two panel concepts and assess their feasibility for a lunar transfer vehicle aerobrake application.

14. SUBJECT TERMS
Aerobrake; Buckling; Sandwich panel; Isogrid panel; Large space structures; Spacecraft design

15. NUMBER OF PAGES
30

16. PRICE CODE
A03

17. SECURITY CLASSIFICATION OF REPORT	18. SECURITY CLASSIFICATION OF THIS PAGE	19. SECURITY CLASSIFICATION OF ABSTRACT	20. LIMITATION OF ABSTRACT
Unclassified	Unclassified		

NSN 7540-01-280-5500

Standard Form 298(Rev. 2-89)
Prescribed by ANSI Std. Z39-18
298-102

NASA-Langley, 1992